pubs.acs.org/acschemicalbiology

Articles

Chemically Modified Bacterial Sacculi as a Vaccine Microparticle Scaffold

Payton A.-B. Weidenbacher, Frances P. Rodriguez-Rivera, Mrinmoy Sanyal, Joshua A. Visser, Jonathan Do, Carolyn R. Bertozzi, and Peter S. Kim*

Cite This: https://doi.org/10.1021/acschembio.2c00140

Read Online

ACCESS | Metrics & More | Article Recommendations | Supporting Information

ABSTRACT: Vaccine scaffolds and carrier proteins increase the immunogenicity of subunit vaccines. Here, we developed, characterized, and demonstrated the efficacy of a novel microparticle vaccine scaffold comprised of bacterial peptidoglycan (PGN), isolated as an entire sacculi. The PGN microparticles contain bio-orthogonal chemical handles allowing for site-specific attachment of immunogens. We first evaluated the purification, integrity, and immunogenicity of PGN microparticles derived from a variety of bacterial species. We then optimized PGN microparticle modification conditions; *Staphylococcus aureus* PGN microparticles containing azido-D-alanine yielded robust conjugation to immunogens. We then demonstrated that this vaccine scaffold elicits comparable immunostimulation to the conventional carrier protein, keyhole limpet hemocyanin (KLH). We further modified the *S. aureus* PGN microparticle to contain the SARS-CoV-2 receptor-binding domain (RBD)—this conjugate vaccine elicited neutralizing antibody titers comparable to those elicited by the KLH-conjugated RBD. Collectively, these findings suggest that chemically modified bacterial PGN microparticles are a conjugatable and biodegradable microparticle scaffold capable of eliciting a robust immune response toward an antigen of interest.

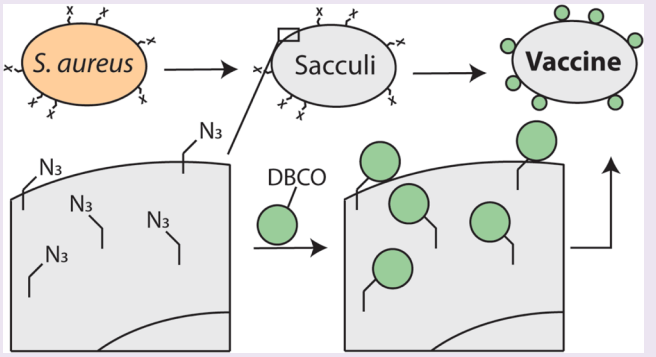

INTRODUCTION

Many protein vaccines, commonly referred to as subunit vaccines, are weakly immunogenic compared to other vaccine types.[1] Subunit vaccines are rapidly degraded and cleared from the body and generally have low intrinsic immunogenic properties.[1] To combat this, adjuvants, carrier proteins, or nanoparticles are often employed.[1] Carrier proteins act by multimerizing subunit vaccines, which promotes B cell receptor cross-linking and uptake by dendritic cells.[2,3] There are clinically tested carrier proteins,[4−6] like keyhole limpet hemocyanin (KLH) isolated directly from keyhole limpets,[1,7] and bovine serum albumin[1] purified by fractionation of bovine plasma,[8] and clinically licensed carriers like diphtheria toxoid[4,9,10] and tetanus toxoid.[4,11] Although anti-carrier immunity[12] can be a concern, carrier proteins have proven effective in amplifying the immunity generated by subunit vaccines. Additionally, inorganic nanoparticles, like metal-based nanoparticles[13] and lipid formulations, have been shown to promote the immune response generated by subunit vaccines. However, their scalability[14,15] and the lack of biodegradability[16−20] have prevented these technologies from being as commonly used as carrier proteins.

In addition to multimerization, nanoparticles and carrier proteins can further promote immunogenicity by acting as an adjuvant. Adjuvants take advantage of innate immune receptors such as toll-like receptors (TLRs), nucleotide-binding oligomerization domain (NOD)-like receptors (NLRs), and other receptors to directly stimulate immune cells.[21−25] Recent work has shown that direct tethering of adjuvants to immunogens is optimal for eliciting a robust immune response.[26−30] As such, many effective carrier proteins are known to activate innate immune receptors. For example, KLH has been shown to be innately immunogenic.[25] Given that the most effective carrier proteins and nanoparticles act by not only multimerizing subunit vaccines but also directly tethering adjuvants to immunogens, we envisioned that a scalable, biodegradable, immunogenic nanoparticle technology could be a very useful tool in the growing arsenal of vaccine carriers.

We proposed that bacterial peptidoglycan (PGN) could fit this brief. PGN is innately immunogenic, naturally biodegradable, and easily purifiable. PGN has been previously used as a vaccine adjuvant in the laboratory[31,32] to stimulate the immune

Received: February 18, 2022
Accepted: April 1, 2022

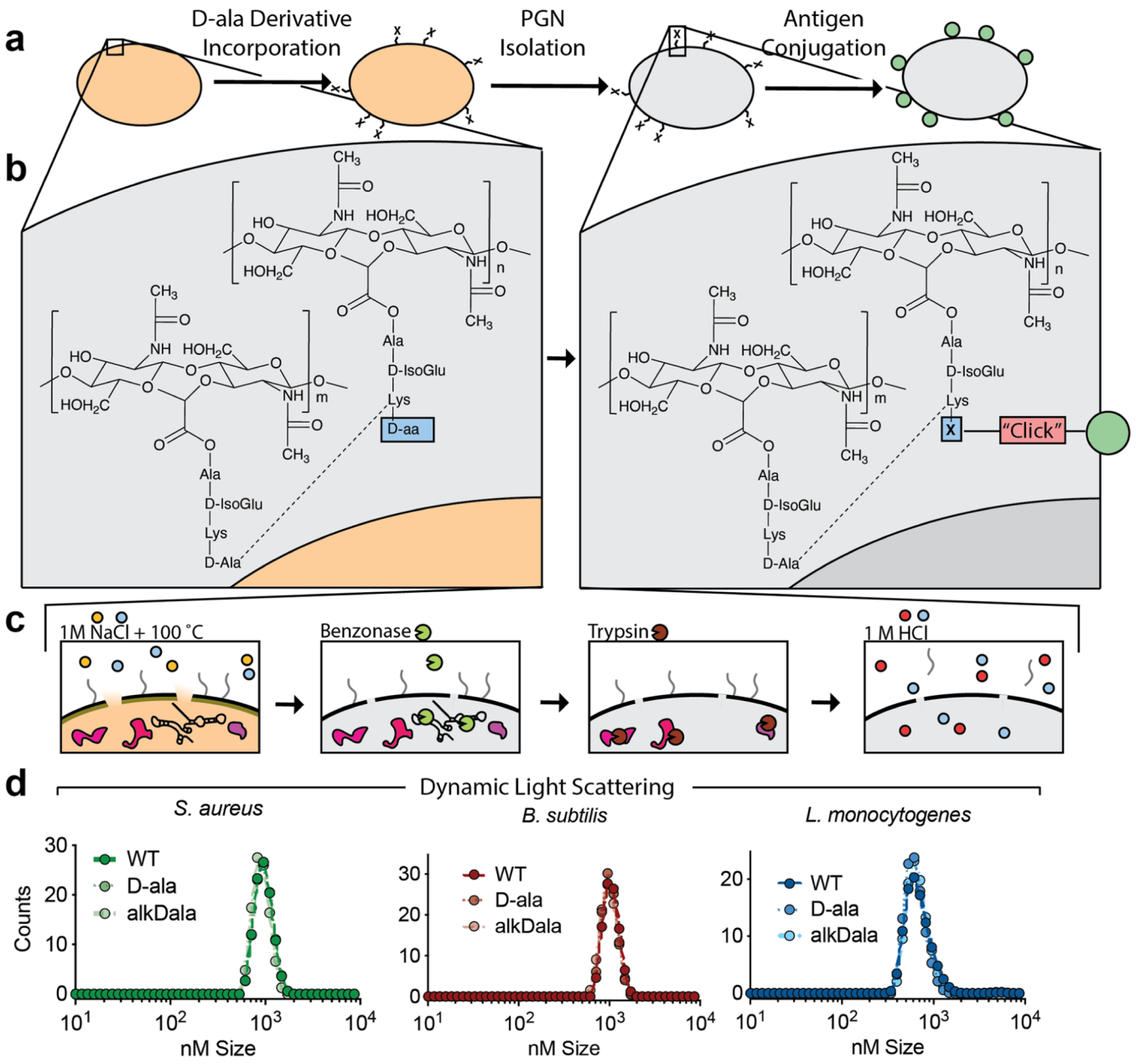

Figure 1. PGN microparticles incorporate unnatural D-aa residues without altering their structures. (a) Schematic for incorporating unnatural D-aa into PGN, purifying it, and conjugating an antigen. Yellow indicates living cell, while gray indicates isolated PGN. (b) Chemical structure of PGN, highlighting the D-ala residue that is likely replaced by the unnatural D-aa residue (X). During conjugation (right), an antigen (green circle) is "clicked" onto the unnatural D-aa. (c) Schematic of PGN microparticle purification from growing bacterial cells. Steps include boiling in 1 M NaCl to burst the membrane and release a variety of intracellular components, followed by benzonase treatment to digest RNA and DNA, trypsin treatment to digest PGN-bound and cellular proteins, and incubation with 1 M HCl to remove wall teichoic acids (Methods). (d) DLS traces of purified PGN microparticles from *S. aureus*, *Bacillus subtilis*, and *L. monocytogenes* containing WT PGN or PGN isolated after growth in broth containing additional D-ala or alkDala.

system through TLR2[33] and NOD1[34] and NOD2 receptors.[34−36] Moreover, PGN is naturally degraded by serum lysozymes[37] and is regularly cleared from the body without significant systemic inflammation.[38,39] These immunogenic properties, coupled with a regular clearance mechanism, make PGN an ideal vaccine adjuvant. Indeed, sortase enzymes have been used previously to covalently conjugate small molecules and proteins to the growing bacterial cell wall for potential vaccine applications,[40−44] further validating the use of PGN as a potential vaccine carrier.

Additionally, there are two key innovations surrounding PGN which we sought to combine to further PGN as a vaccine microparticle. The first is robust and scalable purification techniques which have previously been developed to isolate the entire PGN shell or sacculi (microparticle) from bacterial cells.[45,46] The second is the site-specific metabolic incorporation of clickable D-amino acid (D-aa) derivatives into growing bacterial PGN.[47] These chemical handles have been used previously to covalently attach small molecules like fluorophores,[48,49] pH sensors,[50] and epitopes for antibody recognition[51] to growing or inactivated bacteria. Therefore, we

https://doi.org/10.1021/acschembio.2c00140
ACS Chem. Biol. XXXX, XXX, XXX−XXX

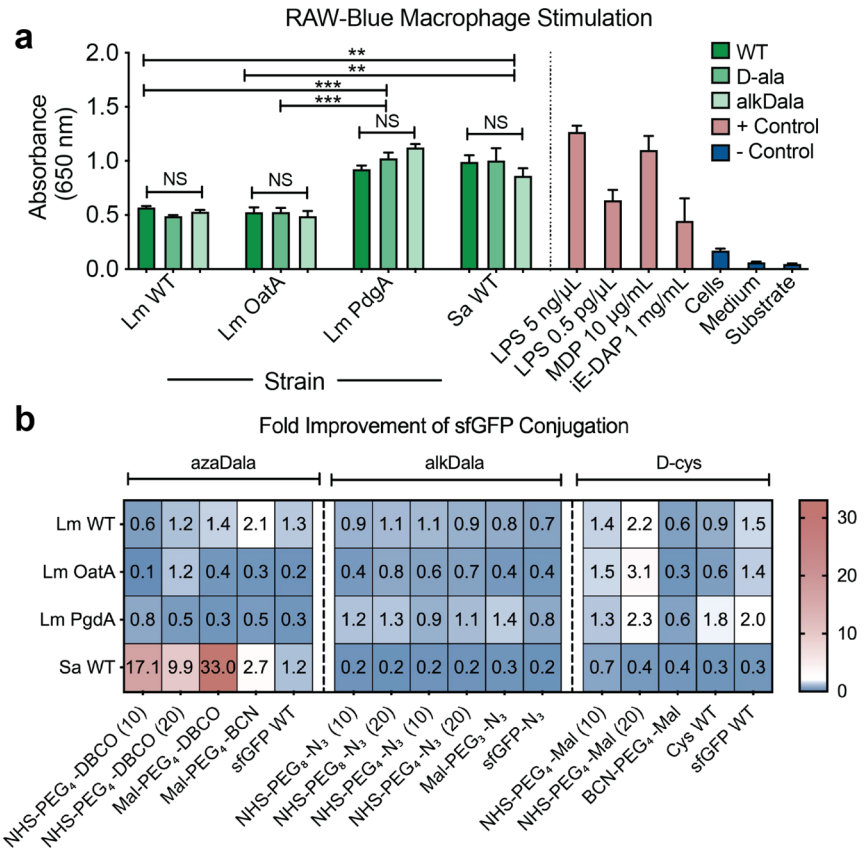

Figure 2. PGN microparticles stimulate macrophages and can conjugate subunit vaccine antigens. (a) RAW-Blue macrophage stimulation assay comparing PGN microparticles isolated from cells grown without unnatural D-aa (WT) or grown with additional D-ala or alkDala. Lm, *L. monocytogenes*; Lm OatA, *L. monocytogenes* with an OatA mutation; Lm PgdA, *L. monocytogenes* with a PdgA mutation; and Sa, *S. aureus*. Positive controls: lipopolysaccharide (LPS), muramyl dipeptide (MDP), and γ-D-Glu-mDAP (iE-DAP). Negative controls: cells with the substrate, medium with the substrate, and the substrate alone. Mean and standard deviations are shown ($n = 3$); each point is the mean of a triplicate measurement from a different day. The highest unpaired *t*-test value for each data set is shown: $^{**}P \leq 0.01$, $^{**}P \leq 0.001$. (b) Heat map of relative conjugation efficiency of isolated PGN microparticles to sfGFP. Relative conjugation efficiency was calculated by dividing the mean fluorescence intensity of modified PGN microparticles by the mean fluorescence intensity of D-ala-PGN microparticles. Numbers in parentheses denote molar equivalents used to non-specifically modify sfGFP.

sought to combine these two advances to produce homogenous, clickable PGN microparticles able to be modified with subunit immunogens.

We isolated and characterized bacterial PGN microparticles following incorporation of an unnatural D-aa. We optimized antigen conjugation to the microparticles and selected *Staphylococcus aureus* PGN modified with azido-D-alanine (azaDala) for subsequent antigen conjugation. We then compared the immunogenicity of the antigen-conjugated PGN microparticles to that of the gold-standard KLH carrier protein in two animal models and with five strains of *S. aureus* PGN microparticles. Finally, we conjugated the SARS-CoV-2 receptor-binding domain (RBD) to the PGN microparticles and established that this RBD-PGN microparticle can elicit neutralizing antibodies against SARS-CoV-2 with similar efficacy to KLH-RBD. Collectively, this work establishes an alternative biodegradable and low-cost vaccine scaffold with tunable immunogenic properties.

RESULTS AND DISCUSSION

Development and Characterization of Chemically Modified PGN Microparticles. We first set out to develop and characterize purified sacculi containing unnatural D-aa derivatives. We incorporated unnatural D-aa derivatives into the PGN shell of growing bacteria and isolated the resultant microparticles[45,46] (Figure 1a). Briefly, growing bacteria were incubated with a D-alanine (D-ala) derivative, which was incorporated into the terminal two positions of the stem peptides in their PGN[47] (Figure 1b). The PGN shell of these bacteria was isolated (Figure 1c) via multiple harsh steps, including boiling in high osmolarity and incubation in 1 M HCl (Methods). The overall scheme was to utilize these purified PGN microparticles to conjugate an immunogen of interest via ligation to the chemical handle on the unnatural D-ala derivative (Figure 1a,b).

To assess whether the incorporation of a modified D-aa residue impacted the PGN structure, we used dynamic light scattering (DLS) to determine the size of the purified sacculi from untreated cells and cells grown in the presence of 1 mM D-ala or 1 mM alkynyl-D-ala (alkDala) (Figure 1d). For the five species of Gram-positive bacteria tested, the microparticles did not substantially differ in size when grown without D-aa derivatives or with 1 mM D-ala or 1 mM alkDala (Figure 1d and Figure S1a). However, purified PGN microparticles of Gram-negative *Escherichia coli* exhibited large variations in size based on growth conditions (Figure S1b). These variations could be due to decreased stability of the thinner PGN shell in Gram-negative[52] *Escherichia coli* compared to the Gram-

https://doi.org/10.1021/acschembio.2c00140
ACS Chem. Biol. XXXX, XXX, XXX−XXX

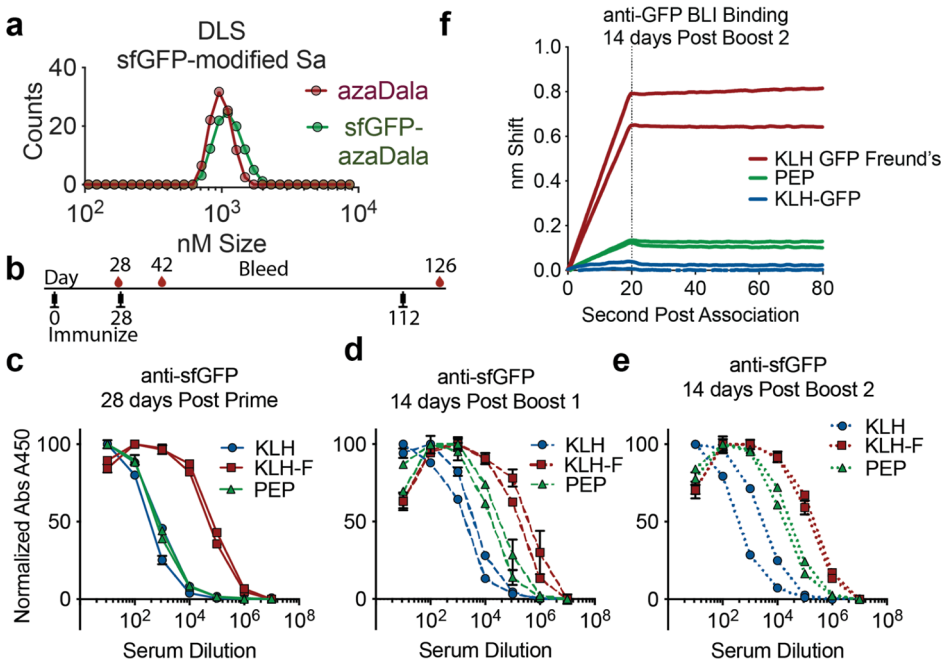

Figure 3. Characterization and immunogenicity of sfGFP-modified PGN microparticles. (a) DLS traces of purified PGN microparticles from azaDala-modified *S. aureus* pre- and post-conjugation with DBCO-modified-sfGFP. (b) Vaccine schedule for the guinea pig immunizations shown in this figure. (c–e) Binding to sfGFP-coated ELISA plates (quantified as net absorbance at 450 nm) for serum isolated at (c) 4 weeks post-prime, (d) 2 weeks post-first boost, and (e) 2 weeks post-second boost. PEP, sfGFP-SA-Aza-Pep. KLH, KLH without the adjuvant. KLH-F, KLH with Freund's adjuvant system. (f) Biolayer interferometry (BLI) of the binding of serum isolated from guinea pigs 2 weeks post-second boost to sfGFP-coated biosensor tips.

positive strains. We also examined genetically modified sacculi in PGN O-acetyltransferase A (OatA) and *N*-acetylglucosamine deacetylase (PgdA) mutants in *Listeria monocytogenes*. These knockout strains of *L. monocytogenes* alter the PGN composition, by removing the enzyme (OatA)[53] responsible for acetylating the C-6 hydroxyl group of the *N*-acetylmuramic acid (MurNAc) residue in the growing PGN or by removing the enzyme responsible for deacetylating (PgdA)[54] the *N*-acetylglucosamine (GlcNAc) residues in the growing PGN. The PGN from both OatA and PgdA knockout cells was previously determined to modify the host immune response[55] and to alter particle degradation by lysozyme-like enzymes.[34,55,56] DLS did not reveal any differences in size for these two strains regardless of growth conditions (Figure S1a).

Having demonstrated that the integrity of Gram-positive PGN shells remained intact after unnatural D-aa incorporation and purification, we next sought to address the immunostimulatory properties of modified PGN microparticles in an NF-κB stimulation reporter cell line. RAW-Blue cells[57] are immortalized murine macrophages that express relevant PGN immune receptors (TLR-2, NOD1, NOD2, etc.) and produce secreted embryonic alkaline phosphatase upon NF-κB activation. We plated macrophages in the presence of PGN microparticles at a 10:33 ratio of cells to PGN and measured NF-κB activation with a colorimetric assay (Methods). We aimed to ensure that PGN microparticles were immunostimulatory, as expected, and that unnatural D-aa incorporation into the PGN microparticles did not influence immunostimulation. Unmodified sacculi and those grown in the presence of additional D-ala or the unnatural amino acid alkDala displayed no significant difference in macrophage activation for most of the Gram-positive samples (Figure 2a). However, *E. coli*, the only Gram-negative species tested here, displayed differing responses (Figure S2), perhaps due to heterogeneity in particle sizes or purity. Given the DLS data (Figure S1b) and this result, *E. coli* was not pursued in future experiments. *Bacillus subtilis* also exhibited markedly different macrophage activation between growth conditions (Figure S2) and was not carried forward for further analysis. Consistent with previous reports, we confirmed that the sacculi isolated from OatA-knockout cells were less immunogenic than sacculi isolated from WT- or PgdA-knockout *L. monocytogenes* strains (Figure 2a).[55] Taken together, these results demonstrate that Gram-positive bacterial PGN can yield homogeneous microparticles that are immunostimulatory.

Optimization of Subunit Protein Conjugation to PGN Microparticles. To evaluate the efficacy of PGN as a vaccine scaffold, we analyzed the ability to conjugate a subunit immunogen to purified sacculi. In order to facilitate comparisons, we utilized the fluorescent, monomeric, 26.8 kDa protein superfolder green fluorescent protein (sfGFP)[58] as a model antigen.[59] To test the conjugation efficiency of sfGFP to the four Gram-positive sacculi (*S. aureus* and three derivatives of *L. monocytogenes*), we purified PGN microparticles containing azido-D-alanine (azaDala), alkDala, or D-cys from these four strains. We then tested the conjugation efficiency of sfGFP derivatives, modified in various ways with the corresponding clickable handles (Figure 2b).[60,61] sfGFP was modified with strained cyclooctynes, azides, or maleimides through *n*-hydroxysuccinimide (NHS) or maleimide chemistries. We analyzed the conjugation efficiency of these click reactions by flow cytometry, comparing the mean fluorescence intensity of the PGN shells with or without corresponding D-aa incorporation (Figures 2b and S3a).

S. aureus PGN modified with azaDala, henceforth referred to as SA Aza-Pep, afforded the highest conjugation efficiency

https://doi.org/10.1021/acschembio.2c00140
ACS Chem. Biol. XXXX, XXX, XXX−XXX

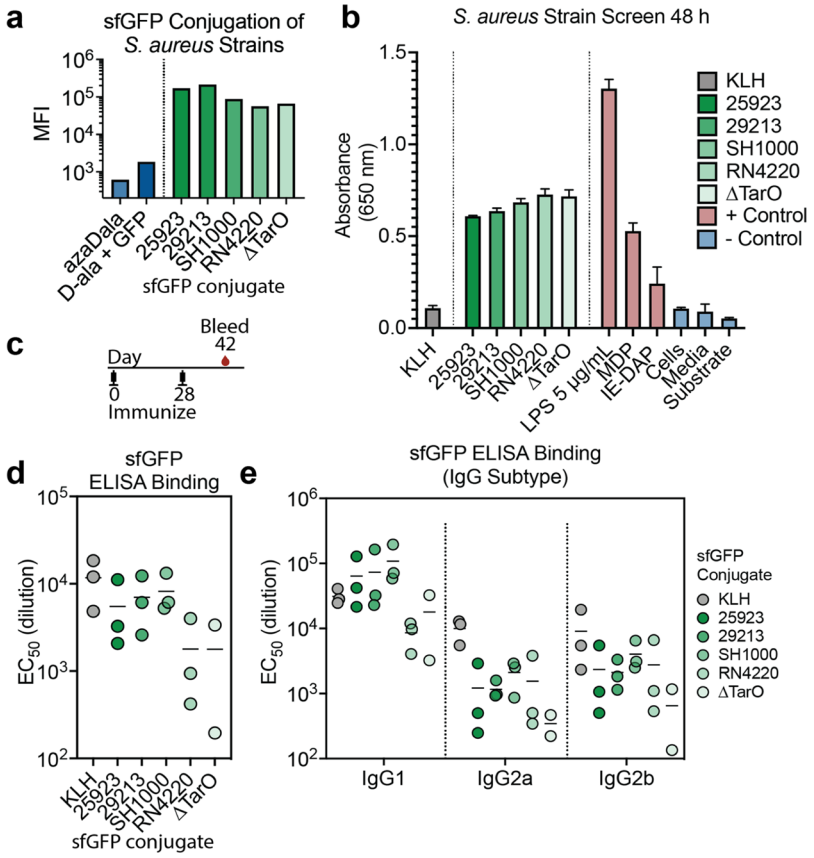

Figure 4. *S. aureus* strain plays a role in overall immune response to PGN microparticles. (a) Mean fluorescence intensity (MFI) of the indicated DBCO sfGFP-conjugated azaDala *S. aureus* strains. (b) RAW-Blue macrophage stimulation assay of sfGFP-modified PGN microparticles from various strains of *S. aureus*. Conditions and analyses are as defined in Figure 2a. (c) Vaccine schedule for the mouse immunizations shown in this figure. (d) Total IgG EC_{50} from ELISA binding titers of mice immunized with sfGFP-conjugated KLH or PGN microparticles from a variety of *S. aureus* strains. (e) ELISA binding titers of specific IgG subtypes from mice immunized with sfGFP-conjugated KLH or PGN microparticles from a variety of *S. aureus* strains.

when conjugated to sfGFP derivatives containing dibenzocyclooctyne (DBCO) functionalities (Figure 2b, left, bottom). The site-specific maleimide-PEG_4-DBCO conjugation to a cysteine at position 3 on sfGFP yielded more effective conjugation than similar NHS-PEG_4-DBCO conjugations (Figure 2b). The resulting maleimide-PEG_4-DBCO conjugation of SA Aza-Pep to sfGFP produced an immunogen henceforth referred to as sfGFP-SA-Aza-Pep. No modification was detected for any condition for the three derivatives of *L. monocytogenes* (Figure 2b), which was surprising because these bacteria readily incorporate unnatural D-aa into their PGN which can be modified by small molecules suggesting that biological processes do not alter unnatural D-aa incorporation.[47] Rather, it is likely that there are fundamental differences in the PGN between *L. monocytogenes* and *S. aureus* which could explain the relative impermeability of the *L. monocytogenes* PGN for the sfGFP protein.[62]

PGN Microparticles as Vaccine Carriers. Given our successful conjugation of a subunit vaccine candidate (sfGFP) to the surface of a *S. aureus* PGN microparticle, we were interested in this microparticle's in vivo efficacy as an immunogen. We sought to compare the immunogenicity of PGN microparticles to that of KLH conjugated to sfGFP. We produced a KLH−sfGFP conjugate using a maleimide-activated KLH in order to also conjugate sfGFP through a cysteine at position 3 and normalized the amount of sfGFP in each immunization sample using a standard sfGFP curve (Figure S3b). Therefore, each immunization sample had an identical amount of fluorescence. Because we were able to determine the molarity of sfGFP in each sample and by knowing the concentration of KLH used in the conjugation or by counting the number of microparticles in a known sample volume by microscopy, we then approximated the number of sfGFP units per KLH (∼21 sfGFP/KLH) and per PGN microparticles (∼250,000 sfGFP/sacculi) (Figure S3c).

Consistent with the addition of sfGFP, DLS indicated a minor increase in size following conjugation (Figure 3a). Given that serum contains lysozyme-like enzymes,[37] we sought to understand the serum stability of these PGN conjugates. We therefore employed fluorescence flow cytometry to detect decreases in both sfGFP fluorescence due to serum proteases and particle degradation due to serum lysozymes. In guinea pig serum, the GFP component of SA-Aza-Pep had a half-life of 4.5 h compared to the 17.7 h for the PGN microparticles (Figure S4a). In rabbit serum, the half-lives were 2.4 and 10.4 h (Figure S4b).

These analyses provided the groundwork for an immunization experiment in guinea pigs with 2.5 μg of sfGFP conjugated to KLH or as sfGFP-SA-Aza-Pep. The immunization protocol contained one boost at week 4 and a second boost at day 112 to investigate long-lived immunity (Figure 3b). We compared the immunization of KLH conjugations with and without

https://doi.org/10.1021/acschembio.2c00140
ACS Chem. Biol. XXXX, XXX, XXX−XXX

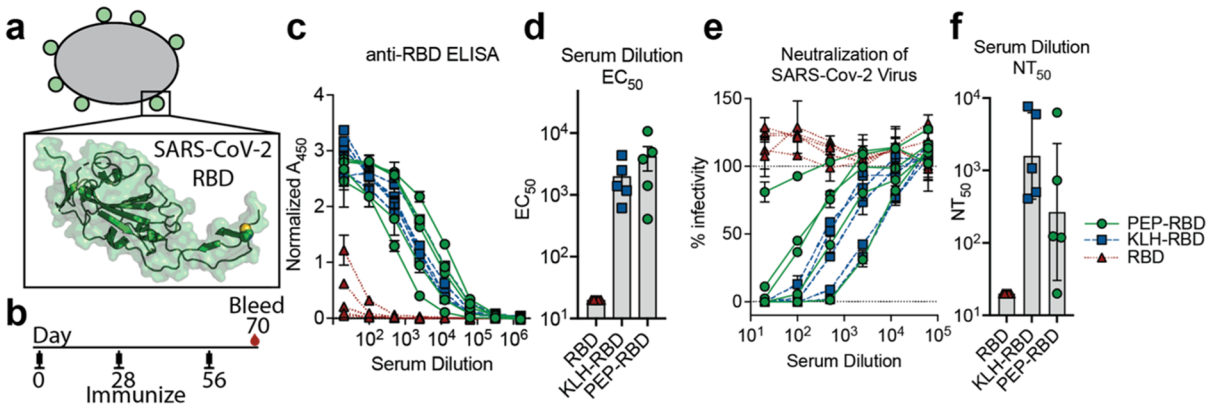

Figure 5. PGN microparticles conjugated with the SARS-CoV-2 RBD elicit a neutralizing antibody response. (a) Schematic of the SARS-CoV-2 RBD conjugated to a PGN microparticle. (b) Vaccination schedule for the mouse immunizations shown in this figure. (c) ELISA binding of serum from mice immunized with SARS-CoV-2-RBD and SARS-CoV-2-RBD conjugates. (d) EC_{50} derived from the curves in (c) (mean and SEM); PEP-RBD is the SARS-CoV-2 RBD conjugated to SH1000 PGN. (e) Neutralization curves of heat-inactivated serum from mice immunized with SARS-CoV-2-RBD conjugates. (f) NT_{50} derived from the curves in (e) (GMT and SD).

Freund's adjuvant system to the adjuvant-free immunization of sfGFP-SA-Aza-Pep. Freund's adjuvant system (Freund's complete adjuvant for the prime, followed by Freund's incomplete adjuvant for the boosts)[63,64] is an extremely robust adjuvant that is not approved for any human or veterinary vaccines but is only used in laboratory settings.[63] Freund's adjuvant contains, among other components, bacterial cell wall fragments from mycobacterium and, therefore, may be stimulating the immune response in a similar way to that of our PGN conjugates.[63,64] We profiled the immune response after the prime (Figure 3c), first boost (Figure 3d), and second boost (Figure 3e). Following a boost, the unadjuvanted sfGFP-SA-Aza-Pep elicited a better immune response than unadjuvanted KLH; however, this response was less robust than with Freund's adjuvant system (Figure 3c,d). Strikingly, following a boost at day 112, sfGFP-SA-Aza-Pep retained a robust response (Figure 3e), demonstrating PGN's ability to elicit an anamnestic immune response. Furthermore, biolayer interferometry, in which the magnitude of the nm shift can be used as a surrogate for binding, indicated the same rank order of binding, with PGN microparticles outperforming KLH (Figure 3f).

***S. aureus* Strain Alters Vaccine Microparticle Efficacy.** Given that the PGN structure is known to be altered based on the bacterial strain,[65] we were next interested in whether the *S. aureus* strains used to produce the PGN microparticles played a role in the host's immune response. We conducted an experiment testing five sfGFP-conjugated *S. aureus* strains for their immunogenicity in mice. We selected two common (Rosenbach)[66] lab strains of *S. aureus* (ATCC: 25923 and 29213), two other common laboratory strains (SH1000[67] and RN4220[68]), and a wall teichoic acid knockout of RN4220 (ΔTarO)[69] for this experiment. Note that our previous experiments had utilized the 25923 strain. Sacculi were isolated from all five strains (Figure S5a) and conjugated using maleimide-PEG_4-DBCO-modified sfGFP. Flow cytometry revealed that the relative conjugation efficiency was similar across all strains tested (Figure 4a). We also confirmed that all versions of PGN from these strains yielded similar macrophage stimulation with RAW-Blue assay, when normalizing for the amount of sfGFP (Figure 4b). Differences in silver staining (Figure S5b) suggested that bacterial components, such as wall teichoic acids, may impact PGN purification efficiency during purification.

PGN strains and KLH were conjugated with sfGFP and then injected into three mice each, while two mice received the ΔTarO conjugate. Mice were immunized at day 0 and boosted at day 28; ELISAs were conducted with serum collected 14 days post-boost (Figure 4c). The immune response was strikingly similar between KLH and PGN, as mice elicited a more robust KLH−sfGFP response and slightly weaker PGN response relative to guinea pigs (Figures 3d and 4d). However, not all *S. aureus* strains elicited a response similar to that elicited by KLH: notably, two strains, RN4220 and the ΔTarO derivative of RN4220, elicited a weaker overall response than the other strains (Figure 4d).

We then profiled the IgG subtypes—a surrogate for immune polarization. Immune polarization is altered by adjuvants[21] and can be profiled by analyzing the relative ratios of IgG1/IgG2 in mice, where IgG1-skewed responses favor Th2-type responses as opposed to a TH1-type response. Given that bacterial infections promote a Th2-type response,[70] it is not surprising that all five sfGFP-PGN conjugate vaccines elicited a preferentially IgG1 response versus IgG2a/b responses (Figure 4e). Other common adjuvants, for example, alum, also promote a Th2-type response.[71] The sfGFP-SH1000-conjugated vaccine appeared to produce the most robust response among the PGN microparticles that we assessed (Figure 4d) and elicited a response in both IgG1 and IgG2a/b (Figure 4e). Additionally, SH1000 contains all four known *N*-acetylglucosaminidases, which hydrolyze the bond between the GlcNAc and MurNAc in the PGN backbone.[72] For this reason, SH1000 PGN was selected for further investigation.

PGN Microparticles as a SARS-CoV-2 RBD Vaccine Carrier. To test whether PGN was a suitable vaccine microparticle for a viral immunogen, we turned to the SARS-CoV-2 RBD (Figure 5a). The RBD[73] has a molecular weight similar to that of sfGFP and was previously shown to produce a skewed IgG1-type response in mice.[74−76] We conjugated the RBD to PGN microparticles through maleimide-PEG_4-DBCO conjugated to Cys538 (Methods; spike numbering). Although the Cys538 position should be a free cystine residue in the RBD construct, previous reports indicated that Cys538 is spontaneously cysteinylated.[77] Therefore, mild tris(2-carboxyethyl) phosphine (TCEP) reduction was utilized to facilitate

https://doi.org/10.1021/acschembio.2c00140
ACS Chem. Biol. XXXX, XXX, XXX−XXX

DBCO conjugation (Methods). Modification was confirmed using the absorbance of DBCO at 310 nm (Figure S6). Biolayer interferometry confirmed that the mildly reduced and DBCO-modified RBD was still bound to conformation-specific antibodies and ACE2 (Figure S7).

Finally, we conjugated the reduced RBD to KLH and the DBCO-modified RBD to SH1000 sacculi and normalized the amount of the RBD in each conjugate. The RBD is not fluorescent; hence, we were unable to use a fluorescence-based standard curve. Instead, we utilized an anti-His tag dot-blot standard curve to bridge the gap between a known concentration of His-tagged sfGFP-modified KLH or PGN microparticles (determined using fluorescence) and His-tagged RBD-modified KLH or PGN microparticles (Figure S8).

We then immunized mice with the unconjugated RBD, KLH-RBD, or SH1000-RBD in phosphate-buffered saline (PBS) with no other adjuvants. Following a prime and two boosts (Figure 5b), the unconjugated RBD elicited a weak response, with only two animals showing any indication of binding and no indication of neutralization[78] (Figure 5c−f). In contrast, both the KLH- and SH1000-conjugated RBDs displayed both binding and neutralization (Figure 5c−f). As with the sfGFP-immunized mice, there was little difference between the KLH- and SH1000-conjugated groups (Figure 5c−f). The improved immunogenicity of the PGN microparticles compared to the unconjugated RBD (Figure 5c−f) demonstrates a clear first step in the development of PGN microparticles as a biodegradable, immunostimulatory, and adaptable vaccine platform. Taken together, this work provides the foundation for the development of PGN microparticles as a novel vaccine scaffold.

DISCUSSION

Here, we demonstrated the utility of PGN microparticles as novel vaccine scaffolds. We established purification protocols and achieved immunostimulation with a variety of PGN microparticles. We demonstrated that *S. aureus* azaDala PGN can conjugate two distinct subunit vaccine candidates, yielding immunostimulation comparable to that achieved with the gold-standard carrier protein KLH. Finally, we demonstrated the efficacy of PGN as a vaccine scaffold for the SARS-CoV-2 RBD: an SH1000-RBD conjugate vaccine elicited neutralizing anti-RBD antibodies at similar efficacy to the KLH-RBD conjugate vaccine.

Subunit vaccines are an attractive alternative to other vaccination methods due to their specificity toward a specific part of the pathogen[1,79] and because their production does not involve the production of large amounts of viruses or bacteria, which can lead to safety concerns. However, the immune response generated by subunit vaccines is often weak (e.g., the response generated to the RBD alone in Figure 5c, red triangles).[80] Therefore, there is a need for technologies that improve the immune response generated by subunit vaccines. Although alternative adjuvants and carrier approaches have been pursued with success,[1,81] there remains an unmet need for immunogenic, easily adaptable carriers that can be produced on scale. PGN microparticles have been produced on a large scale from liters of culture[82] and constitute a scalable vaccine microparticle, as showcased here.

In combination with the data presented herein, there are simple and effective next steps that can improve PGN microparticles in future studies. They could easily be combined with a variety of other adjuvants[83] or stabilizing agents,[81] further increasing their immunogenicity. Moreover, it is possible to incorporate multiple distinct clickable handles into individual microparticles (by simply growing the cells in broth containing an additional D-aa). This allows for the production of PGN microparticles that can simultaneously contain the antigen, clicked to one handle, and a multiplicity of additional TLR agonists,[26] T-cell epitopes,[84] or cancer neoantigens[85] conjugated to the orthogonal handle.[26,86]

Finally, in contrast to the inorganic nanoparticles, like gold or silver nanoparticles,[13] that are used in vaccination, PGN is a native substrate for many endogenous enzymes and is therefore readily biodegradable.[16,87] Meanwhile, the composition of PGN and its overall stability during the harsh purification process (Figure 1c) suggest that PGN would benefit from the same advantages as inorganic scaffolds, like their solvency and pH stability, while mitigating their risks. Bacteria are commonly lyophilized and shipped at room temperature, and therefore, it is quite likely that PGN microparticles could afford the same stability and ease of storage. Given the current global limitations on cold-chain storage, stable PGN microparticles could offer an alternative scaffold that is amenable to large-scale distribution. The advantages of their production, ease of purification, stability, and innate immune properties render PGN microparticles an ideal addition to the growing arsenal of vaccine nanoparticles.

In conclusion, our PGN microparticle scaffold is a unique, biodegradable nanoparticle capable of eliciting an immune response similar to that elicited by commonly used carrier proteins like KLH. In mice, RBD-PGN microparticles elicited a neutralizing response to SARS-CoV-2. PGN microparticles are a potentially scalable subunit vaccine conjugation platform whose stability could avoid cold-chain transportation requirements.

METHODS

PGN Production and Isolation. Wildtype (WT), OatA-, or PgdA-expressing bacteria were grown to saturation in LB medium. This suspension was diluted 1:10,000 into 3−4 mL of LB containing the 1 mM unnatural D-ala derivative and grown overnight to saturation. Cultures were harvested by centrifugation at 13,000*g* for 1 min and washed twice with 1× PBS. For isolation, cells were resuspended in 1 M NaCl (for Gram-positive cells) or 0.1 M Tris/HCl pH 7 + 0.25% SDS (for Gram-negative cells) and boiled for 30 min at 100 °C. These suspensions were washed twice with ddH_2O, resuspended in 500 μL of ddH_2O, and sonicated in a water bath for 30 min. Five hundred microliters of Tris buffer pH 7.4 with 1 μL of benzonase (Sigma) was added to each sample and incubated at 37 °C for 1 h. Thirty microliters of trypsin (HyClone 0.25%) was added to each sample and incubated at 37 °C for 1 h. Samples were then boiled at 100 °C for 5 min and washed twice with ddH_2O. Finally, samples were incubated in 1 mL of 1 M HCl for 4 h at 37 °C, washed with ddH_2O until their pH was approximately neutral, and then spun down at 13,000*g* and resuspended into 1× PBS for use in conjugation reactions. All experiments in Figures 1−3 were conducted with a single preparation of bacterial PGN. Future experiments were conducted with two additional preparations of isolated PGN. Batch to batch variability was low (~MFI for sfGFP conjugation was ~10^5 in measured preparations).

Dynamic Light Scattering. DLS measurements were taken on a Malvern Zetasizer Nano S. One hundred microliters of the PGN suspension was added to a 70 μL disposable cuvette, and the temperature was equilibrated to 25 °C for at least 2 min prior to sample measurement.

RAW-Blue NF-kB Activity Assay. RAW-Blue cells were purchased from InvivoGen, and the macrophages were maintained as described by the manufacturer. Briefly, cells were maintained in

https://doi.org/10.1021/acschembio.2c00140
ACS Chem. Biol. XXXX, XXX, XXX−XXX

DMEM medium supplemented with 4.5 g/L glucose, 10% fetal bovine serum (FBS), and 100 μg/mL Normocin (InvivoGen) and Zeocin (InvivoGen). One hundred eighty microliters of cells were plated at 550,000 cells/mL in a 96-well dish with 20 μL of PGN, suspended in endotoxin-free H_2O. The amount of PGN per sample was previously quantified via serial dilution and imaged via confocal microscopy to achieve 3.3 PGN per macrophage in each well. For testing the *S. aureus* strains, 3 μL of the sample (10 μg/mL sfGFP) was used. The assays were conducted in the same medium except that the FBS in this assay was heat-inactivated. Plates were incubated for 48 h at 37 °C and 5% CO_2. A 50 μL sample of the supernatant was taken and added to 150 μL of QUANTI-Blue (InvivoGen). This mixture was incubated in 96-well flat-bottom plates for 30 min at 37 °C before quantification with a spectrophotometer (BioTek Synergy HT Microplate Reader) at 650 nm. Experiments were conducted in triplicate of triplicate. Mean and standard deviations of the mean from the three experiments are shown. Data were analyzed with GraphPad Prism 9 using an unpaired *t*-test.

sfGFP Expression. The gene encoding sfGFP was cloned into a pET28b vector with a C-terminal hexa-His tag. For all constructs in which a maleimide was conjugated or a free cysteine was utilized, a Cys residue was incorporated at position 3. The sfGFP-N_3 construct containing a genetically encoded azido-phenyl alanine (pET22b-T5-sfGFP* and pUltra-Poly) was generously supplied by Professor Peter Schultz at Scripps. All cells were grown in 2XYT medium and induced at OD_{600} 0.6−0.8. In the case of sfGFP-N_3, 2XYT was supplemented with 1 mM azido-phenyl alanine (Chem Impex) dissolved in H_2O, solubilized dropwise with NaOH (conc), and filtered with a 0.22 μm filter. Cells were induced with 1 mM IPTG, and the protein was expressed for 4 h at 37 °C with shaking.

sfGFP Purification. *E. coli* cells were harvested by centrifugation for 10 min at 5000*g* and lysed via sonication. Sonicated samples were spun again at 13,000*g* for 1 h, and GFP was purified from cell lysates through Ni-NTA purification (HisPur Ni-NTA resin, Thermo Fisher). sfGFP used for conjugation experiments was buffer exchanged into PBS. For all other experiments, sfGFP was run over endotoxin removal resin (Pierce) and purified FPL (Superdex 200).

RBD and Monoclonal Antibody Expression. RBD, monoclonal antibodies, and soluble human ACE2-Fc were expressed and purified from Expi293F cells (Thermo Fisher). Expi293F cells were cultured in 66% Freestyle/33% Expi medium (Thermo Fisher) and grown in TriForest polycarbonate shaking flasks at 37 °C in 8% CO_2. One day prior to transfection, cells were spun down at 300*g* and resuspended to a density of 3×10^6 cells/mL in fresh medium. The next day, cells were diluted and transfected at a density of approximately $3-4 \times 10^6$ cells/mL. Transfection mixtures were made by adding maxi-prepped DNA, culture medium, and FectoPRO (Polyplus) to cells to a ratio of 0.5−0.8 μg:100 μL:1.3 μL:900 μL. For example, for a 100 mL transfection, 50−80 μg of DNA was added to 10 mL of culture medium, and then, 130 μL of FectoPRO was added to that mixture. Following mixing and a 10 min incubation, the resultant transfection cocktail was added to 90 mL of cells. The cells were harvested 3−5 days after transfection by spinning the cultures at >7000*g* for 15 min. Supernatants were filtered using a 0.22 μm filter.

RBD Purification. The RBD was purified using HisPur Ni-NTA resin (Thermo Fisher). Expi293F cell supernatants were diluted with 1/3 volume wash buffer (20 mM imidazole, 20 mM HEPES pH 7.4, and 150 mM NaCl), and the Ni-NTA resin was added to diluted cell supernatants. The RBD was incubated at 4 °C with stirring overnight. Resin/supernatant mixtures were added to chromatography columns for gravity flow purification. The resin in the column was washed with wash buffer (20 mM imidazole, 20 mM HEPES pH 7.4, and 150 mM NaCl), and the RBD was eluted with 250 mM imidazole, 20 mM HEPES pH 7.4, and 105 mM NaCl. Column elutions were concentrated using centrifugal concentrators (10 kDa cutoff for the RBD), followed by size-exclusion chromatography on an AKTA Pure system (Cytiva). AKTA Pure FPLC with a Superdex 6 Increase gel filtration column (S6) was used for purification. One milliliter of the sample was injected using a 2 mL loop and run over the S6, which had been preequilibrated in degassed 20 mM HEPES and 150 mM NaCl prior to use. Biotinylated antigens were not purified using the AKTA.

Protein Purification (Fc Tag). Anti-RBD IgGs and hFc-Ace2 fusions were purified using a 5 mL MAbSelect SuRe Prism column on the AKTA Pure FPLC (Cytiva). Filtered cell supernatants were diluted with 1/10 volume of 10× PBS. The AKTA system was equilibrated with 1× PBS for A1, 100 mM glycine pH 2.8 for A2, 0.5 M NaOH for B1, 1× PBS for the buffer line, and H_2O for the sample lines. The protocol involved washing the column with A1, then loading the sample in Sample line 1 until air was detected in the air sensor of the sample pumps, followed by five column volume washes with A1, and elution of the sample by flowing of 20 mL of A2 (directly into a 50 mL conical containing 2 mL of 1 M Tris pH 8.0) followed by five column volumes of A1, B1, and A1. The resultant Fc-containing samples were concentrated using 50 or 100 kDa cutoff centrifugal concentrators (Amicon). Proteins were buffer exchanged using a PD-10 column (Sephadex) that had been preequilibrated into 20 mM HEPES and 150 mM NaCl. IgG-ACE2 fusions were further purified using the S6 column on the AKTA as described above.

Screening sfGFP Conjugation Conditions to Isolate PGN. Previously prepared sfGFP was conjugated through maleimide (two molar equivalents in 1× PBS), through *N*-hydroxysuccinimide (respective number of molar equivalents shown above in 1× PBS), or left unconjugated. After conjugation, all samples were buffer exchanged into 1× PBS and diluted to 1 mg/mL. PGN isolated as described above was spun down at 13,000*g* and resuspended in 1 mg/mL solutions of sfGFP derivatives with their respective clickable handles. Cu-free click reactions and thiol-reactive samples were incubated for 1 h at room temperature. To the Cu click samples of a preformed complex of BTTAA (33 mM, two molar equivalents) and $CuSO_4$ (16.5 μM, 1 equivalent) was added freshly prepared 100 mM sodium ascorbate. Reactions were incubated at room temperature and then spun down and washed six times with PBS.

sfGFP Conjugation to PGN Microparticles and KLH. Samples were prepared as mentioned above using dibenzocyclooctyne (DBCO)-conjugated sfGFP incubated at 12 mg/mL with *S. aureus* PGN (ATCC 25923 or other strains as described; from 4 mL of culture) containing an azido-D-ala. PGN samples were incubated and rotated for 96 h at room temperature and purified by spinning down and resuspending in PBS six times. Alternatively, Cys-3-GFP was mixed 1:1 each 10 mg/mL with maleimide KLH (Imject). KLH samples were prepared per the manufacturer's recommendation (2 h in 1× PBS). KLH was purified away from GFP using successive passes through a 100 kDa concentrator (Amicon) until no unconjugated GFP was seen in solution. Quantification of the GFP concentration in each sample was done using a standard curve of GFP fluorescence (GraphPad Prism Version 9).

RBD Reduction Reaction and Conjugation to Maleimide-DBCO. The previously prepared SARS-CoV-2 RBD was reduced by the addition of one molar equivalent TCEP and left to incubate at room temperature for 1 h. Samples were then buffer exchanged into PBS using a PD-10 column (Cytiva). Following reduction, the RBD was mixed with two molar equivalents of maleimide-PEG_4-DBCO and left to react for 2 h at room temperature. A PD-10 column was used to isolate the reacted RBD from unreacted maleimide.

RBD Conjugation to Isolated PGN. The previously prepared SARS-CoV-2 RBD conjugated with maleimide-PEG_4-DBCO was mixed at 2 mg/mL to SH100 PGN microparticles (PGN microparticles isolated from 4 mL of SH1000 *S. aureus* culture). Prior to conjugation, the RBD was sterile filtered using a 0.22 μm filter. SH1000 PGN microparticles were boiled at 100 °C for 20 min to sterilize them, as they could not be filtered due to their size. These mixed reactions were rocked at room temperature for 3 days and then spun down (13,000*g*) and resuspended six times with PBS.

GFP Conjugation Evaluation. sfGFP-conjugated samples were analyzed by flow cytometry (BD Accuri C6), and the mean fluorescence intensity of the conjugated samples was divided by that of the unconjugated samples (exact sample conditions as mentioned above, but PGN lacked the clickable handle) and is

https://doi.org/10.1021/acschembio.2c00140
ACS Chem. Biol. XXXX, XXX, XXX−XXX

plotted in Figure 2. Samples compared were turquoise (clicked) to orange (unclicked) (Figure S3a). Data were analyzed using flowJo.

Quantification of RBD Conjugation. To quantify the amount of the RBD in solution, we developed a standard curve dot blot using His-tagged sfGFP and the RBD. sfGFP-conjugated KLH or PGN microparticles (of a known sfGFP concentration, as determined with a standard curve) were dotted in duplicate on a nitrocellulose membrane (1.8 μL dots, Thermo Fisher) in twofold dilutions. Unknown concentrations of RBD-conjugated KLH or PGN microparticles were also dotted in duplicate. In a final lane, unmodified PGN microparticles were dotted as a control. An anti-his dot blot was conducted as follows. The blot was dried for 15 min in a fume hood. Following drying, 10 mL of a 1× PBST + 5% blotting grade blocker (Bio-Rad) was added for 10 min. Two microliters of the mouse anti-hexa His antibody (BioLegend) was added to the 10 mL sample and incubated for 1 h at room temperature. Blots were washed 16 times with 9 mL of PBST. Ten milliliters of the 1× PBST + 5% blotting grade blocker with 2 μL of anti-mouse IgG1 (Abcam) was added and incubated for 1 h at room temperature. Blots were washed 16 times with 9 mL of PBST, developed using the Pierce ECL Western blotting substrate and imaged using a GE Amersham imager 600. Dots were quantified using the gel analysis protocol in Fiji (Version 1.0, ImageJ), and curves were fitted, and unknown concentrations were evaluated using a linear regression in GraphPad Prism 8.4.1.

Guinea Pig and Rabbit Serum Stability Assays. Samples of sfGFP-conjugated PGN microparticles (ATCC: 25923) were incubated in 25% guinea pig or rabbit serum and 75% RPMI with shaking at 37 °C for 62 h. At 0, 1, 10, 24, 38, 48, and 62 h, 100 μL of samples was taken and flash frozen using liquid nitrogen. Following isolation of the final timepoint, samples were thawed simultaneously, added to a v-bottom plate, and analyzed by flow cytometry (BD Accuri C6). Gates were drawn to encompass PGN microparticles, and the mean fluorescence intensity and raw counts were collected. Curves were fit using a one-phase decay in GraphPad Prism 8.4.1.

Mutanolysin Digestion and Silver Stain Analysis. Ten microliters of 10 μg/mL sfGFP-conjugated PGN microparticles in 1× PBS was digested with 10 ng of mutanolysin (Sigma) followed by incubation overnight with shaking at 37 °C. Following digestion, a silver stain was conducted (Pierce, Thermo Fisher). The gel was run in clean running buffer (Bio-Rad), washed five times in ddH_2O, fixed with 30% ethanol:10% acetic acid for 15 min, and replaced with the same solution for another 15 min. The gel was then washed with 10% ethanol and ddH_2O twice for 5 min. Sensitizer working solution was made (one part Silver Stain Sensitizer and 500 parts ultrapure water) and incubated with the gel for 1 min. The gel was then washed twice for 1 min with ddH_2O. Next, the gel was incubated for 30 min in Stain Working Solution (one part Silver Stain Enhancer with 50 parts Silver Stain). The gel was washed twice in ddH_2O and then added to Developer Working Solution (one part Silver Stain Enhancer with 50 parts Silver Stain Developer) and incubated until protein bands appeared. This reaction was quenched with 5% acetic acid, washed once quickly, and incubated in 5% acetic acid for 10 min.

Guinea Pig Immunizations. Male guinea pigs were given intramuscular immunizations containing 2.5 μg of GFP in 100 μL of each sample (Josman LLC). Prior to immunizations, samples were mixed 1:1 with 1× PBS (PGN and KLH without Freund's samples) or 1:1 with Freund's complete adjuvant (primary) and Freund's incomplete adjuvant (subsequent immunizations) for KLH-GFP Freund's samples. Immunizations occurred on Day 0, 28, and 112, and bleeds were conducted on Day 0, 28, 42, and 126. Animal studies were conducted according to the regulations set forth by USDA under the Animal Welfare Act (7 U.S.C. 2131 et seq.) and the policies set forth by the National Institutes of Health through the Office of Laboratory Animal Welfare.

Mouse Immunizations. Samples of sfGFP-PGN microparticles from a variety of species and SARS-CoV-2 RBD-PGN microparticles from SH1000 or comparable KLH controls were prepared in 1× PBS at a concentration of 10 μg/mL of sfGFP or the SARS-CoV-2 RBD. The GFP concentration in each sample was quantified using a standard curve of GFP fluorescence; the RBD was quantified with a standard curve produced by dot blot (described above). One microgram of GFP or the RBD (in 100 μL) of each sample was immunized intramuscularly into BALB/C mice (Jackson Laboratory). Immunizations and bleeds occurred following the schedules described in the figures.

Biolayer Interferometry. Guinea pig serum was analyzed using an Octet Red96. Serum was directly diluted into 1:100 into PBST + bovine serum albumin. Streptavidin biosensors were loaded with 100 nM biotinylated sfGFP that had been biotinylated using maleimide-peg11-biotin (EZ-Link) as described above. Sensor tips were baselined in a 1:100 dilution of pre-immune serum, left to associate in 1:100 post-immune serum, and then dissociated back in the pre-immune serum. Plots were made using GraphPad Prism 8.4.1.

Serum ELISAs. ELISAs were done essentially as previously described.[79] Briefly, plates (Maxisorb) were coated in 50 μL of 5 μg/mL sfGFP or the RBD for 2 h at room temperature. Plates were washed three times with 1× PBST and then blocked with 1× PBST with 0.5% bovine serum albumin (GFP) or ChonBlock (RBD) for at least 1 h at room temperature. Plates were washed once with 1× PBST, 50 μL of serial dilutions of guinea pig or mouse serum in 1× PBST was added to the plate for 1 h at room temperature, and the plates were washed three times with 1× PBST. An anti-guinea pig horseradish peroxidase secondary antibody (Abcam) at a 1:10,000 dilution or anti-mouse or anti-mouse IgG1/IgG2a/IgG2b (Abcam) in 1× PBST was added to each well and incubated for 1 h at room temperature. Finally, plates were washed four times with 1× PBST, and 50 μL of 1-Step Turbo TMB-ELISA Substrate Solution (Thermo Fisher Scientific) was added to each well. Plates were quenched with 50 μL of 2 M H_2SO_4 and read on a spectrophotometer. Data were visualized, and EC_{50} was calculated using GraphPad Prism 8.4.1.

SARS-CoV-2 Neutralization. Target cells used for infection in viral neutralization assays were from a HeLa cell line stably overexpressing the SARS-CoV-2 receptor, ACE2, and the protease known to process SARS-CoV-2, TMPRSS2. Production of this cell line is described in detail by Rogers et al., 2020,[78,88] with the addition of stable TMPRSS2 incorporation. ACE2/TMPRSS2/HeLa cells were plated at 5000 cells per well on white-walled, clear-bottom 96-well plates (Thermo Fisher Scientific) 1 day prior to infection. On the day of the assay, dilutions of serum were made into sterile D10 medium [500 mL of DMEM + 10% FBS, 5 mL of L-glutamate, penicillin, and streptomycin (5 mL of 100×), and 10 mM HEPES] to a final volume of 60 μL. For viral neutralization assays, mouse serum was centrifuged at 2000*g* for 15 min and heat inactivated for 30 min at 56 °C. Samples were run in technical duplicate in each experiment. All other wells contained only D10 medium. A virus mixture was made containing the virus of interest (e.g., SARS-CoV-2 with a 21-amino acid deletion at the C terminus), D10 medium, and polybrene (final concentration 5 μg/mL). Virus dilutions into medium were selected such that a suitable signal would be obtained in the virus-only wells (luminescence > 10,000 RLU). Sixty microliters of this virus mixture was added to each of the inhibitor dilution to a final volume of 120 μL in each well. Virus-only wells contained 60 μL of D10 medium and 60 μL of the virus mixture. Cell-only wells contained 120 μL of D10 medium. The serum dilution/virus mixture was left to incubate for 1 h at 37 °C. Following incubation, the medium was removed from the cells on the plates made 1 day prior, replaced with 100 μL of inhibitor/virus dilutions, and incubated at 37 °C for approximately 48 h. Infectivity was read out by measuring luciferase levels 48 h post-infection: 50 μL of medium was removed from all cells, and then, cells were lysed by adding 50 μL of BriteLite assay readout solution (PerkinElmer) into each well. Luminescence values were measured with a BioTek Synergy HT Microplate Reader (BioTek). Each plate was normalized by averaging cell-only (0% infectivity) and virus-only (100% infectivity) wells. Normalized values were fit with a three-parameter non-linear regression inhibitor curve in GraphPad Prism 9.1.0 to obtain IC_{50} values.

SARS-CoV-2 Spike Pseudotyped Lentivirus Production. Viral transfections were done in HEK293T cells using a calcium phosphate transfection reagent. Six million cells were seeded in D10 medium in 10 cm plates 1 day prior to transfection. A five-plasmid system was

https://doi.org/10.1021/acschembio.2c00140
ACS Chem. Biol. XXXX, XXX, XXX−XXX

used for viral production.[78] The Spike vector contained the 21-amino acid truncated form of the SARS-CoV-2 Spike sequence from the Wuhan-Hu-1 strain of SARS-CoV-2 (GenBank: BCN86353.1). The plasmids were added to D10 medium in the following amounts: 10 μg of pHAGE-Luc2-IRS-ZsGreen, 3.4 μg of FL Spike, 2.2 μg of HDM-Hgpm2, 2.2 μg of HDM-Tat1b, and 2.2 μg of pRC-CMV-Rev1b in a final volume of 1 mL; subsequently, 30 μL of Bio T was added. Transfection reactions were incubated for 10 min at room temperature and then filled to 10 mL with D10 medium. These samples were added slowly to plated cells without medium. After 24 h (post-transfection), medium was removed and replaced with fresh D10 medium. Viral supernatants were harvested 72 h post-transfection by spinning at 300*g* for 5 min followed by filtering through a 0.45 μm filter. Viral stocks were aliquoted and stored at −80 °C until further use.

■ ASSOCIATED CONTENT

Supporting Information

The Supporting Information is available free of charge at https://pubs.acs.org/doi/10.1021/acschembio.2c00140.

Additional data on Gram-negative bacteria, serum stability, characterization of variant strains, SARS-CoV-2 conjugation evaluation, and conjugation measurement methodology for sfGFP and the SARS-CoV-2 RBD (PDF)

■ AUTHOR INFORMATION

Corresponding Author

Peter S. Kim − *Stanford ChEM-H, Stanford University, Stanford, California 94305, United States; Department of Biochemistry, School of Medicine, Stanford University, Stanford, California 94305, United States; Chan Zuckerberg Biohub, San Francisco, California 94158, United States;* orcid.org/0000-0001-6503-4541; Email: kimpeter@stanford.edu

Authors

Payton A.-B. Weidenbacher − *Stanford ChEM-H, Stanford University, Stanford, California 94305, United States; Department of Chemistry, Stanford University, Stanford, California 94305, United States;* orcid.org/0000-0002-7692-0458

Frances P. Rodriguez-Rivera − *Stanford ChEM-H, Stanford University, Stanford, California 94305, United States; Department of Chemistry, Stanford University, Stanford, California 94305, United States;* orcid.org/0000-0003-0651-8639

Mrinmoy Sanyal − *Stanford ChEM-H, Stanford University, Stanford, California 94305, United States; Department of Biochemistry, School of Medicine, Stanford University, Stanford, California 94305, United States*

Joshua A. Visser − *Stanford ChEM-H, Stanford University, Stanford, California 94305, United States; Department of Chemistry, Stanford University, Stanford, California 94305, United States*

Jonathan Do − *Stanford ChEM-H, Stanford University, Stanford, California 94305, United States; Department of Biochemistry, School of Medicine, Stanford University, Stanford, California 94305, United States*

Carolyn R. Bertozzi − *Stanford ChEM-H, Stanford University, Stanford, California 94305, United States; Department of Chemistry, Stanford University, Stanford, California 94305, United States;* orcid.org/0000-0003-4482-2754

Complete contact information is available at: https://pubs.acs.org/10.1021/acschembio.2c00140

Notes

The authors declare the following competing financial interest(s): P.A.-B.W., F.P.R.R., C.R.B., and P.S.K. are named as inventors on a provisional patent application applied for by Stanford University and the Chan Zuckerberg Biohub on chemically modified bacterial peptidoglycan compositions and uses thereof.

■ ACKNOWLEDGMENTS

We thank J. Bloom and A. Greaney for plasmids and cells related to viral neutralization assays. The CMV/R expression vectors for IgG production were received from the NIH AIDS Reagent Program. The pET22b-T5-sfGFP* and pUltra-Poly plasmids were generously gifted from P. Schultz. This work was supported by the Virginia & D.K. Ludwig Fund for Cancer Research, the Frank Quattrone and Denise Foderaro Family Research Fund, and the Chan Zuckerberg Biohub.

■ REFERENCES

(1) Vartak, A.; Sucheck, S. Recent Advances in Subunit Vaccine Carriers. *Vaccines* **2016**, *4*, 12−18.

(2) Pati, R.; Shevtsov, M.; Sonawane, A. Nanoparticle Vaccines Against Infectious Diseases. *Front. Immunol.* **2018**, *9*, 2224.

(3) Veneziano, R.; Moyer, T. J.; Stone, M. B.; Wamhoff, E.-C.; Read, B. J.; Mukherjee, S.; Shepherd, T. R.; Das, J.; Schief, W. R.; Irvine, D. J.; et al. Role of Nanoscale Antigen Organization on B-Cell Activation Probed Using DNA Origami. *Nat. Nanotechnol.* **2020**, *15*, 716−723.

(4) Pichichero, M. E. Protein Carriers of Conjugate Vaccines: Characteristics, Development, and Clinical Trials. *Hum. Vaccines Immunother.* **2013**, *9*, 2505−2523.

(5) Slovin, S. F.; Ragupathi, G.; Musselli, C.; Fernandez, C.; Diani, M.; Verbel, D.; Danishefsky, S.; Livingston, P.; Scher, H. I. Thomsen-Friedenreich (TF) Antigen as a Target for Prostate Cancer Vaccine: Clinical Trial Results with TF Cluster (c)-KLH plus QS21 Conjugate Vaccine in Patients with Biochemically Relapsed Prostate Cancer. *Cancer Immunol. Immunother.* **2005**, *54*, 694−702.

(6) Miles, D.; Roché, H.; Martin, M.; Perren, T. J.; Cameron, D. A.; Glaspy, J.; Dodwell, D.; Parker, J.; Mayordomo, J.; Tres, A.; et al. Phase III Multicenter Clinical Trial of the Sialyl-TN (STn)-Keyhole Limpet Hemocyanin (KLH) Vaccine for Metastatic Breast Cancer. *Oncologist* **2011**, *16*, 1092−1100.

(7) Robin Harris, J.; Gebauer, W.; Söhngen, S. M.; Markl, J. Keyhole Limpet Haemocyanin (KLH): Purification of Intact KLH1 through Selective Dissociation of KLH2. *Micron* **1995**, *26*, 201−212.

(8) Balkani, S.; Shamekhi, S.; Raoufinia, R.; Parvan, R.; Abdolalizadeh, J. Purification and Characterization of Bovine Serum Albumin Using Chromatographic Method. *Adv. Pharm. Bull.* **2016**, *6*, 651−654.

(9) Reisinger, K. S.; Baxter, R.; Block, S. L.; Shah, J.; Bedell, L.; Dull, P. M. Quadrivalent Meningococcal Vaccination of Adults: Phase III Comparison of an Investigational Conjugate Vaccine, MenACWY-CRM, with the Licensed Vaccine, Menactra. *Clin. Vaccine Immunol.* **2009**, *16*, 1810−1815.

(10) Lepow, M. L.; Samuelson, J. S.; Gordon, L. K. Safety and Immunogenicity of Haemophilus Influenzae Type B Polysaccharide-Diphtheria Toxoid Conjugate Vaccine in Adults. *J. Infect. Dis.* **1984**, *150*, 402−406.

(11) Schneerson, R.; Robbins, J. B.; Parke, J. C., Jr.; Bell, C.; Schlesselman, J. J.; Sutton, A.; Wang, Z.; Schiffman, G.; Karpas, A.; Shiloach, J. Quantitative and Qualitative Analyses of Serum Antibodies Elicited in Adults by Haemophilus Influenzae Type b and Pneumococcus Type 6A Capsular Polysaccharide-Tetanus Toxoid Conjugates. *Infect. Immun.* **1986**, *52*, 519−528.

(12) Ertekin, Ö.; Akçael, E.; Kocaağa, H.; Öztürk, S. Biological Activity of the Carrier as a Factor in Immunogen Design for Haptens. *Molecules* **2018**, *23*, 2977.
(13) Marques Neto, L. M.; Kipnis, A.; Junqueira-Kipnis, A. P. Role of Metallic Nanoparticles in Vaccinology: Implications for Infectious Disease Vaccine Development. *Front. Immunol.* **2017**, *8*, 239.
(14) Yoo, J.-W.; Irvine, D. J.; Discher, D. E.; Mitragotri, S. Bio-Inspired, Bioengineered and Biomimetic Drug Delivery Carriers. *Nat. Rev. Drug Discovery* **2011**, *10*, 521−535.
(15) Poon, C.; Patel, A. A. Organic and Inorganic Nanoparticle Vaccines for Prevention of Infectious Diseases. *Nano Express* **2020**, *1*, 012001.
(16) Zhao, L.; Seth, A.; Wibowo, N.; Zhao, C.-X.; Mitter, N.; Yu, C.; Middelberg, A. P. J. Nanoparticle Vaccines. *Vaccine* **2014**, *32*, 327−337.
(17) Al Zaki, A. Z.; Hui, J. Z.; Higbee, E.; Tsourkas, A. Biodistribution, Clearance, and Toxicology of Polymeric Micelles Loaded with 0.9 or 5 Nm Gold Nanoparticles. *J. Biomed. Nanotechnol.* **2015**, *11*, 1836−1846.
(18) Sonavane, G.; Tomoda, K.; Makino, K. Biodistribution of Colloidal Gold Nanoparticles after Intravenous Administration: Effect of Particle Size. *Colloids Surf., B* **2008**, *66*, 274−280.
(19) Balasubramanian, S. K.; Jittiwat, J.; Manikandan, J.; Ong, C.-N.; Yu, L. E.; Ong, W.-Y. Biodistribution of Gold Nanoparticles and Gene Expression Changes in the Liver and Spleen after Intravenous Administration in Rats. *Biomaterials* **2010**, *31*, 2034−2042.
(20) Longmire, M.; Choyke, P. L.; Kobayashi, H. Clearance Properties of Nano-Sized Particles and Molecules as Imagin Agents: Consideration and Caveats. *Nanomedicine* **2008**, *3*, 703−717.
(21) Pulendran, B.; Arunachalam, P. S.; O'Hagan, D. T. Emerging Concepts in the Science of Vaccine Adjuvants. *Nat. Rev. Drug Discovery* **2021**, *20*, 454−475.
(22) Medzhitov, R.; Janeway, C. A. Innate Immunity: The Virtues of a Nonclonal System of Recognition. *Cell* **1997**, *91*, 295−298.
(23) Curtis, J. E.; Hersh, E. M.; Harris, J. E.; McBride, C.; Freireich, E. J. The Human Primary Immune Response to Keyhole Limpet Haemocyanin: Interrelationships of Delayed Hypersensitivity, Antibody Response and in Vitro Blast Transformation. *Clin. Exp. Immunol.* **1970**, *6*, 473−491.
(24) Harris, J. R.; Markl, J. u. r. Keyhole Limpet Hemocyanin: Molecular Structure of a Potent Marine Immunoactivator. *Eur. Urol.* **2000**, *37*, 24−33.
(25) Yasuda, K.; Ushio, H. Keyhole Limpet Hemocyanin Induces Innate Immunity via Syk and Erk Phosphorylation. *EXCLI J.* **2016**, *15*, 474−481.
(26) Tom, J. K.; Dotsey, E. Y.; Wong, H. Y.; Stutts, L.; Moore, T.; Davies, D. H.; Felgner, P. L.; Esser-Kahn, A. P. Modulation of Innate Immune Responses via Covalently Linked TLR Agonists. *ACS Cent. Sci.* **2015**, *1*, 439−448.
(27) Huleatt, J. W.; Jacobs, A. R.; Tang, J.; Desai, P.; Kopp, E. B.; Huang, Y.; Song, L.; Nakaar, V.; Powell, T. J. Vaccination with Recombinant Fusion Proteins Incorporating Toll-like Receptor Ligands Induces Rapid Cellular and Humoral Immunity. *Vaccine* **2007**, *25*, 763−775.
(28) Shirota, H.; Sano, K.; Kikuchi, T.; Tamura, G.; Shirato, K. Regulation of Murine Airway Eosinophilia and Th2 Cells by Antigen-Conjugated CpG Oligodeoxynucleotides as a Novel Antigen-Specific Immunomodulator. *J. Immunol.* **2000**, *164*, 5575−5582.
(29) Shirota, H.; Sano, K.; Hirasawa, N.; Terui, T.; Ohuchi, K.; Hattori, T.; Shirato, K.; Tamura, G. Novel Roles of CpG Oligodeoxynucleotides as a Leader for the Sampling and Presentation of CpG-Tagged Antigen by Dendritic Cells. *J. Immunol.* **2001**, *167*, 66−74.
(30) Phillipps, K. S. M.; Wykes, M. N.; Liu, X. Q.; Brown, M.; Blanchfield, J.; Toth, I. A Novel Synthetic Adjuvant Enhances Dendritic Cell Function. *Immunology* **2009**, *128*, e582−e588.
(31) Webster, R. G.; Glezen, W. P.; Hannoun, C.; Laver, W. G. Potentiation of the Immune Response to Influenza Virus Subunit Vaccines. *J. Immunol.* **1977**, *119*, 2073−2077.
(32) Adam, A.; Ciorbaru, R.; Ellouz, F.; Petit, J.-F.; Lederer, E. Adjuvant Activity of Monomeric Bacterial Cell Wall Peptidoglycans. *Biochem. Biophys. Res. Commun.* **1974**, *56*, 561−567.
(33) Iyer, J. K.; Coggeshall, K. M. Primary Innate Immune Cells Respond Efficiently to Polymeric Peptidoglycan but Not to Peptidoglycan Monomers. *J. Immunol.* **2011**, *186*, 3841−3845.
(34) Clarke, T. B.; Davis, K. M.; Lysenko, E. S.; Zhou, A. Y.; Yu, Y.; Weiser, J. N. Recognition of Peptidoglycan from the Microbiota by Nod1 Enhances Systemic Innate Immunity. *Nat. Med.* **2010**, *16*, 228−231.
(35) Philpott, D. J.; Sorbara, M. T.; Robertson, S. J.; Croitoru, K.; Girardin, S. E. NOD Proteins: Regulators of Inflammation in Health and Disease. *Nat. Rev. Immunol.* **2014**, *14*, 9−23.
(36) Wolf, A. J.; Underhill, D. M. Peptidoglycan Recognition by the Innate Immune System. *Nat. Rev. Immunol.* **2018**, *18*, 243−254.
(37) Tullio, V.; Spaccapelo, R.; Polimeni, M. Lysozymes in the Animal Kingdom. *Human and Mosquito Lysozymes: Old Molecules for New Approaches Against Malaria*; Springer, 2015; Vol. *35*, pp 45−57.
(38) Royet, J.; Dziarski, R. Peptidoglycan Recognition Proteins: Pleiotropic Sensors and Effectors of Antimicrobial Defences. *Nat. Rev. Microbiol.* **2007**, *5*, 264−277.
(39) Chaput, C.; Boneca, I. G. Peptidoglycan Detection by Mammals and Flies. *Microbes Infect.* **2007**, *9*, 637−647.
(40) Gautam, S.; Gniadek, T. J.; Kim, T.; Spiegel, D. A. Exterior Design: Strategies for Redecorating the Bacterial Surface with Small Molecules. *Trends Biotechnol.* **2013**, *31*, 258−267.
(41) Nelson, J. W.; Chamessian, A. G.; McEnaney, P. J.; Murelli, R. P.; Kazmiercak, B. I.; Spiegel, D. A. A Biosynthetic Strategy for Re-Engineering the Staphylococcus Aureus Cell Wall with Non-Native Small Molecules. *ACS Chem. Biol.* **2010**, *5*, 1147−1155.
(42) Kumari, P.; Bowmik, S.; Paul, S. K.; Biswas, B.; Banerjee, S. K.; Murty, U. S.; Ravichandiran, V.; Mohan, U. Sortase A: A Chemoenzymatic Approach for the Labeling of Cell Surfaces. *Biotechnol. Bioeng.* **2021**, *118*, 4577−4589.
(43) Marraffini, L. A.; Dedent, A. C.; Schneewind, O. Sortases and the Art of Anchoring Proteins to the Envelopes of Gram-Positive Bacteria. *Microbiol. Mol. Biol. Rev.* **2006**, *70*, 192−221.
(44) Garufi, G.; Wang, Y.-T.; Oh, S.-Y.; Maier, H.; Missiakas, D. M.; Schneewind, O. Sortase-Conjugation Generates a Capsule Vaccine That Protects Guinea Pigs against Bacillus Anthracis. *Vaccine* **2012**, *30*, 3435−3444.
(45) Kühner, D.; Stahl, M.; Demircioglu, D. D.; Bertsche, U. From Cells to Muropeptide Structures in 24 h: Peptidoglycan Mapping by UPLC-MS. *Sci. Rep.* **2014**, *4*, 7494.
(46) Zhou, X.; Cegelski, L. Nutrient-Dependent Structural Changes in S. Aureus Peptidoglycan Revealed by Solid-State NMR Spectroscopy. *Biochemistry* **2012**, *51*, 8143−8153.
(47) Siegrist, M. S.; Whiteside, S.; Jewett, J. C.; Aditham, A.; Cava, F.; Bertozzi, C. R. D-Amino Acid Chemical Reporters Reveal Peptidoglycan Dynamics of an Intracellular Pathogen. *ACS Chem. Biol.* **2013**, *8*, 500−505.
(48) Shieh, P.; Siegrist, M. S.; Cullen, A. J.; Bertozzi, C. R. Imaging Bacterial Peptidoglycan with Near-Infrared Fluorogenic Azide Probes. *Proc. Natl. Acad. Sci. U.S.A.* **2014**, *111*, 5456−5461.
(49) Hsu, Y.-P.; Hall, E.; Booher, G.; Murphy, B.; Radkov, A. D.; Yablonowski, J.; Mulcahey, C.; Alvarez, L.; Cava, F.; Brun, Y. V.; et al. Fluorogenic D-Amino Acids Enable Real-Time Monitoring of Peptidoglycan Biosynthesis and High-Throughput Transpeptidation Assays. *Nat. Chem.* **2019**, *11*, 335−341.
(50) Kamariza, M.; Shieh, P.; Ealand, C. S.; Peters, J. S.; Chu, B.; Rodriguez-Rivera, F. P.; Babu Sait, M. R.; Treuren, W. V.; Martinson, N.; Kalscheuer, R.; et al. Rapid Detection of Mycobacterium Tuberculosis in Sputum with a Solvatochromic Trehalose Probe. *Sci. Transl. Med.* **2018**, *10*, No. eaam6310.
(51) Fura, J. M.; Sabulski, M. J.; Pires, M. M. D-Amino Acid Mediated Recruitment of Endogenous Antibodies to Bacterial Surfaces. *ACS Chem. Biol.* **2014**, *9*, 1480−1489.
(52) Silhavy, T. J.; Kahne, D.; Walker, S. The Bacterial Cell Envelope. *Cold Spring Harbor Perspect. Biol.* **2010**, *2*, a000414.

https://doi.org/10.1021/acschembio.2c00140
ACS Chem. Biol. XXXX, XXX, XXX−XXX

(53) Sychantha, D.; Jones, C. S.; Little, D. J.; Moynihan, P. J.; Robinson, H.; Galley, N. F.; Roper, D. I.; Dowson, C. G.; Howell, P. L.; Clarke, A. J. In Vitro Characterization of the Antivirulence Target of Gram-Positive Pathogens, Peptidoglycan O-Acetyltransferase A (OatA). *PLoS Pathog.* **2017**, *13*, No. e1006667.
(54) Rismondo, J.; Wamp, S.; Aldridge, C.; Vollmer, W.; Halbedel, S. Stimulation of PgdA-Dependent Peptidoglycan N-Deacetylation by GpsB-PBP A1 in Listeria Monocytogenes. *Mol. Microbiol.* **2018**, *107*, 472−487.
(55) Bera, A.; Herbert, S.; Jakob, A.; Vollmer, W.; Götz, F. Why Are Pathogenic Staphylococci so Lysozyme Resistant? The Peptidoglycan O-Acetyltransferase OatA Is the Major Determinant for Lysozyme Resistance of Staphylococcus Aureus. *Mol. Microbiol.* **2005**, *55*, 778−787.
(56) Boneca, I. G.; Dussurget, O.; Cabanes, D.; Nahori, M.-A.; Sousa, S.; Lecuit, M.; Psylinakis, E.; Bouriotis, V.; Hugot, J.-P.; Giovannini, M.; et al. Critical Role for Peptidoglycan N-Deacetylation in Listeria Evasion from the Host Innate Immune System. *Pnas* **2007**, *104*, 997−1002.
(57) Lewis, R. E.; Liao, G.; Young, K.; Douglas, C.; Kontoyiannis, D. P. Macrophage Reporter Cell Assay for Screening Immunopharmacological Activity of Cell Wall-Active Antifungals. *Antimicrob. Agents Chemother.* **2014**, *58*, 1738−1743.
(58) Pédelacq, J.-D.; Cabantous, S.; Tran, T.; Terwilliger, T. C.; Waldo, G. S. Engineering and Characterization of a Superfolder Green Fluorescent Protein. *Nat. Biotechnol.* **2006**, *24*, 79−88.
(59) Gambotto, A.; Dworacki, G.; Cicinnati, V.; Kenniston, T.; Steitz, J.; Tüting, T.; Robbins, P.; DeLeo, A. Immunogenicity of Enhanced Green Fluorescent Protein (EGFP) in BALB/c Mice: Identification of an H2-Kd-Restricted CTL Epitope. *Gene Ther.* **2000**, *7*, 2036−2040.
(60) Sletten, E. M.; Bertozzi, C. R. Bioorthogonal Chemistry: Fishing for Selectivity in a Sea of Functionality. *Angew. Chem., Int. Ed.* **2009**, *48*, 6974−6998.
(61) Xiao, H.; Nasertorabi, F.; Choi, S.-h.; Han, G. W.; Reed, S. A.; Stevens, R. C.; Schultz, P. G. Exploring the Potential Impact of an Expanded Genetic Code on Protein Function. *Proc. Natl. Acad. Sci. U.S.A.* **2015**, *112*, 6961−6966.
(62) Vollmer, W.; Blanot, D.; De Pedro, M. A. Peptidoglycan Structure and Architecture. *FEMS Microbiol. Rev.* **2008**, *32*, 149−167.
(63) Stils, H. F. Adjuvants and Antibody Production: Dispelling the Myths Associated with Freund's Complete and Other Adjuvants. *ILAR J.* **2005**, *46*, 280−293.
(64) Freund, J.; Casals, J.; Hosmer, E. P. Sensitization and Antibody Formation after Injection of Tubercle Bacilli and Paraffin Oil. *Proc. Soc. Exp. Biol. Med.* **1937**, *37*, 509−513.
(65) Barzilai, A.; Hyatt, A. C.; Hodes, D. S. Demonstration of Differences between Strains of Staphylococcus Aureus by Peptidoglycan Fingerprinting. *J. Infect. Dis.* **1984**, *150*, 583−588.
(66) Rosenbach, A. J. F. *Mikro-Organismen Bei Den Wund-Infections-Krankheiten Des Menschen*; J.F. Bergmann, 1884; Vol. 2.
(67) Horsburgh, M. J.; Aish, J. L.; White, I. J.; Shaw, L.; Lithgow, J. K.; Foster, S. J. SigmaB Modulates Virulence Determinant Expression and Stress Resistance: Characterization of a Functional RsbU Strain Derived from Staphylococcus Aureus 8325-4. *J. Bacteriol.* **2002**, *184*, 5457−5467.
(68) Kreiswirth, B. N.; Löfdahl, S.; Betley, M. J.; O'Reilly, M.; Schlievert, P. M.; Bergdoll, M. S.; Novick, R. P. The Toxic Shock Syndrome Exotoxin Structural Gene Is Not Detectably Transmitted by a Prophage. *Nature* **1983**, *305*, 709−712.
(69) Wang, H.; Gill, C. J.; Lee, S. H.; Mann, P.; Zuck, P.; Meredith, T. C.; Murgolo, N.; She, X.; Kales, S.; Liang, L.; et al. Discovery of Wall Teichoic Acid Inhibitors as Potential Anti-MRSA β-Lactam Combination Agents. *Chem. Biol.* **2013**, *20*, 272−284.
(70) D'Elios, M. M.; Benagiano, M.; Della Bella, C.; Amedei, A. T-Cell Response to Bacterial Agents. *J. Infect. Dev. Countries* **2011**, *5*, 640−645.
(71) Marrack, P.; McKee, A. S.; Munks, M. W. Towards an Understanding of the Adjuvant Action of Aluminium. *Nat. Rev. Immunol.* **2009**, *9*, 287−293.
(72) Wheeler, R.; Turner, R. D.; Bailey, R. G.; Salamaga, B.; Mesnage, S.; Mohamad, S. A. S.; Hayhurst, E. J.; Horsburgh, M.; Hobbs, J. K.; Foster, S. J. Bacterial Cell Enlargement Requires Control of Cell Wall Stiffness Mediated by Peptidoglycan Hydrolases. *MBio* **2015**, *6*, No. e00660.
(73) Amanat, F.; Stadlbauer, D.; Strohmeier, S.; Nguyen, T. H. O.; Chromikova, V.; McMahon, M.; Jiang, K.; Arunkumar, G. A.; Jurczyszak, D.; Polanco, J.; et al. A Serological Assay to Detect SARS-CoV-2 Seroconversion in Humans. *Nat. Med.* **2020**, *26*, 1033−1036.
(74) Powell, A. E.; Zhang, K.; Sanyal, M.; Tang, S.; Weidenbacher, P. A.; Li, S.; Pham, T. D.; Pak, J. E.; Chiu, W.; Kim, P. S. A Single Immunization with Spike-Functionalized Ferritin Vaccines Elicits Neutralizing Antibody Responses against SARS-CoV-2 in Mice. *ACS Cent. Sci.* **2021**, *7*, 183−199.
(75) Dalvie, N. C.; Rodriguez-Aponte, S. A.; Hartwell, B. L.; Tostanoski, L. H.; Biedermann, A. M.; Crowell, L. E.; Kaur, K.; Kumru, O. S.; Carter, L.; Yu, J.; et al. Engineered SARS-CoV-2 Receptor Binding Domain Improves Manufacturability in Yeast and Immunogenicity in Mice. *Proc. Natl. Acad. Sci. U.S.A.* **2021**, *118*, No. e2106845118.
(76) Siriwattananon, K.; Manopwisedjaroen, S.; Shanmugaraj, B.; Rattanapisit, K.; Phumiamorn, S.; Sapsutthipas, S.; Trisiriwanich, S.; Prompetchara, E.; Ketloy, C.; Buranapraditkun, S.; et al. Plant-Produced Receptor-Binding Domain of SARS-CoV-2 Elicits Potent Neutralizing Responses in Mice and Non-Human Primates. *Front. Plant Sci.* **2021**, *12*, 1−15.
(77) Valdes-Balbin, Y.; Santana-Mederos, D.; Quintero, L.; Fernández, S.; Rodriguez, L.; Sanchez Ramirez, B.; Perez-Nicado, R.; Acosta, C.; Méndez, Y.; Ricardo, M. G.; et al. SARS-CoV-2 RBD-Tetanus Toxoid Conjugate Vaccine Induces a Strong Neutralizing Immunity in Preclinical Studies. *ACS Chem. Biol.* **2021**, *16*, 1223−1233.
(78) Crawford, K. H. D.; Eguia, R.; Dingens, A. S.; Loes, A. N.; Malone, K. D.; Wolf, C. R.; Chu, H. Y.; Tortorici, M. A.; Veesler, D.; Murphy, M.; et al. Protocol and Reagents for Pseudotyping Lentiviral Particles with SARS-CoV-2 Spike Protein for Neutralization Assays. *Viruses* **2020**, *12*, 513.
(79) Weidenbacher, P. A.; Kim, P. S. Protect, Modify, Deprotect (PMD): A Strategy for Creating Vaccines to Elicit Antibodies Targeting a Specific Epitope. *Proc. Natl. Acad. Sci. U.S.A.* **2019**, *116*, 9947−9952.
(80) Haynes, B. F.; Kelsoe, G.; Harrison, S. C.; Kepler, T. B. B-Cell-Lineage Immunogen Design in Vaccine Development with HIV-1 as a Case Study. *Nat. Biotechnol.* **2012**, *30*, 423−433.
(81) Roth, G. A.; Gale, E. C.; Alcántara-Hernández, M.; Luo, W.; Axpe, E.; Verma, R.; Yin, Q.; Yu, A. C.; Lopez Hernandez, H.; Maikawa, C. L.; et al. Injectable Hydrogels for Sustained Codelivery of Subunit Vaccines Enhance Humoral Immunity. *ACS Cent. Sci.* **2020**, *6*, 1800−1812.
(82) Tong, G.; Pan, Y.; Dong, H.; Pryor, R.; Wilson, G. E.; Schaefer, J. Structure and Dynamics of Pentaglycyl Bridges in the Cell Walls of Staphylococcus Aureus by 13C-15N REDOR NMR. *Biochemistry* **1997**, *36*, 9859−9866.
(83) Glenny, A. T.; Pope, C. G.; Waddington, H.; Wallace, U. Immunological Notes. XVII-XXIV. *J. Pathol. Bacteriol.* **1926**, *29*, 31−40.
(84) Patronov, A.; Doytchinova, I. T-Cell Epitope Vaccine Design by Immunoinformatics. *Open Biol.* **2013**, *3*, 120139.
(85) Blass, E.; Ott, P. A. Advances in the Development of Personalized Neoantigen-Based Therapeutic Cancer Vaccines. *Nat. Rev. Clin. Oncol.* **2021**, *18*, 215−229.
(86) Lynn, G. M.; Laga, R.; Darrah, P. A.; Ishizuka, A. S.; Balaci, A. J.; Dulcey, A. E.; Pechar, M.; Pola, R.; Gerner, M. Y.; Yamamoto, A.; et al. In Vivo Characterization of the Physicochemical Properties of Polymer-Linked TLR Agonists That Enhance Vaccine Immunogenicity. *Nat. Biotechnol.* **2015**, *33*, 1201−1210.

https://doi.org/10.1021/acschembio.2c00140
ACS Chem. Biol. XXXX, XXX, XXX−XXX

(87) Irvine, D. J.; Hanson, M. C.; Rakhra, K.; Tokatlian, T. Synthetic Nanoparticles for Vaccines and Immunotherapy. *Chem. Rev.* **2015**, *115*, 11109−11146.
(88) Rogers, T. F.; Zhao, F.; Huang, D.; Beutler, N.; Burns, A.; He, W.-t.; Limbo, O.; Smith, C.; Song, G.; Woehl, J.; et al. Isolation of Potent SARS-CoV-2 Neutralizing Antibodies and Protection from Disease in a Small Animal Model. *Science* **2020**, *369*, 956−963.

https://doi.org/10.1021/acschembio.2c00140
ACS Chem. Biol. XXXX, XXX, XXX−XXX

Supporting Information

Chemically Modified Bacterial Sacculi as a Vaccine Microparticle Scaffold

Payton A.-B. Weidenbacher[†,‡], Frances P. Rodriguez-Rivera[†,‡], Mrinmoy Sanyal[†,§], Joshua A. Visser[†,‡], Jonathan Do[†,§], Carolyn R. Bertozzi[†,‡], Peter S. Kim*[†,§,¶]

[†]Stanford ChEM-H, Stanford University, Stanford, California 94305, United States; [‡]Department of Chemistry, Stanford University, Stanford, California 94305, United States; [§]Department of Biochemistry, School of Medicine, Stanford University, Stanford, California 94305, United States; [¶]Chan Zuckerberg Biohub, San Francisco, California 94158, United States

*kimpeter@stanford.edu

SI Fig 1a

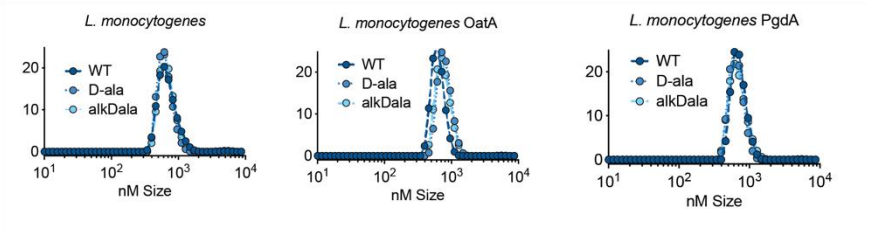

SI Fig 1b

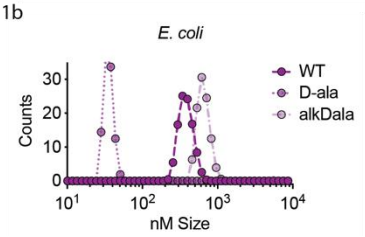

SI Figure 1 – DLS traces of *L. monocytogenes* derivatives look consistent while *E. Coli* looks irregular. (A) DLS traces of purified PGN microparticles from *L. monocytogenes* containing "wildtype" growth conditions (WT) PGN (no D-aa in the growth medium), PGN isolated from bacteria grown in the presence of additional D-ala or alkDala, or PGN isolated from *L. monocytogenes* (expressing OatA or PgdA) without or with D-ala or alkDala. (B) DLS traces of purified PGN microparticles from *E. coli* containing WT PGN, PGN isolated from bacteria grown in the presence of additional D-ala, or PGN isolated from bacteria grown in the presence of alkDala.

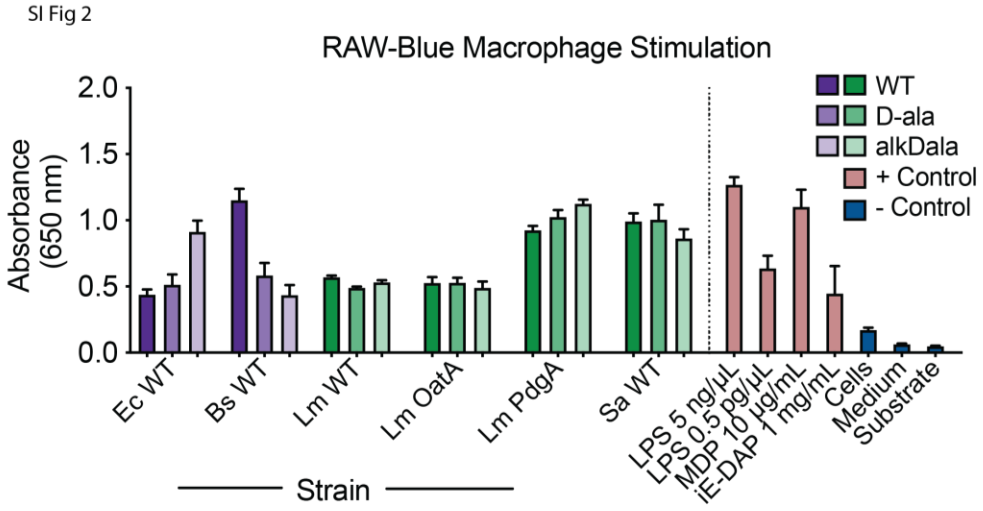

SI Figure 2 – RAW-Blue macrophage stimulation assay comparing isolated PGN microparticles with the no additional D-aa added or with the addition of D-ala or alkDala. Gram-negative *Escherichia coli* (Ec) and Gram-positive *Bacillus subtilis* (Bs) show higher heterogeneity than Gram-positive *Listeria monocytogenes* (Lm) or *Staphylococcus aureus* (Sa). LPS, lipopolysaccharide; MDP, muramyl dipeptide; IE-DAP, γ-D-Glu-mDAP. Each value is plotted as the average of three means from a triplicate measurement

SI Fig 3a

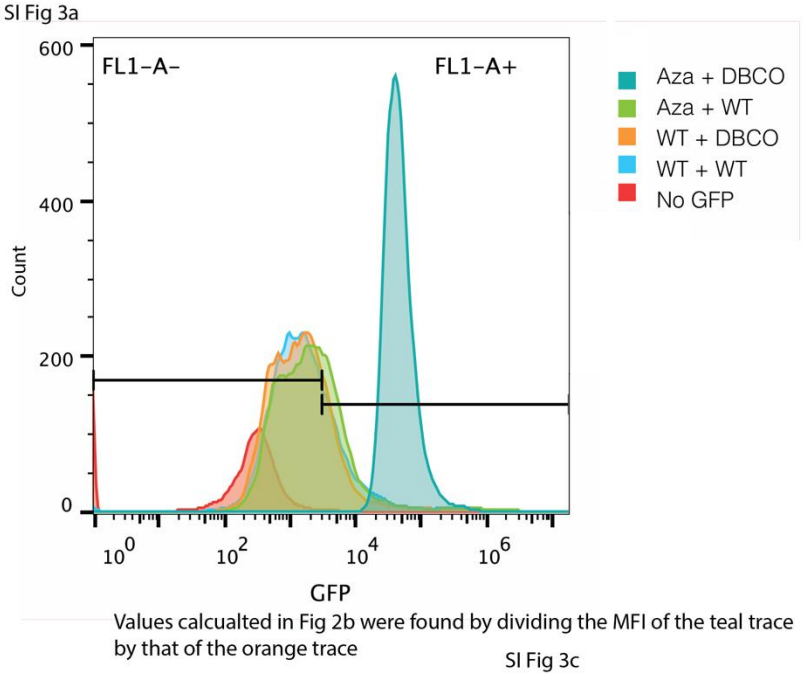

Values calcualted in Fig 2b were found by dividing the MFI of the teal trace by that of the orange trace

SI Fig 3b

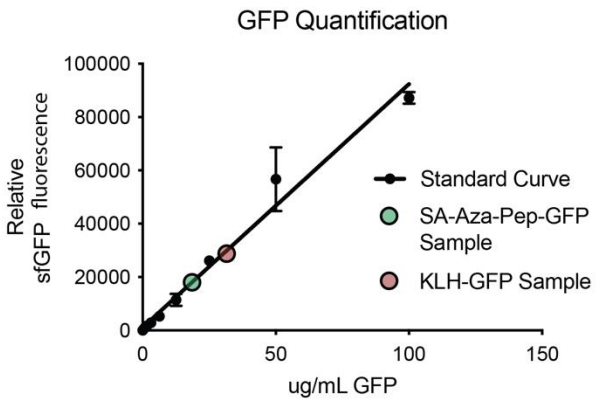

SI Fig 3c

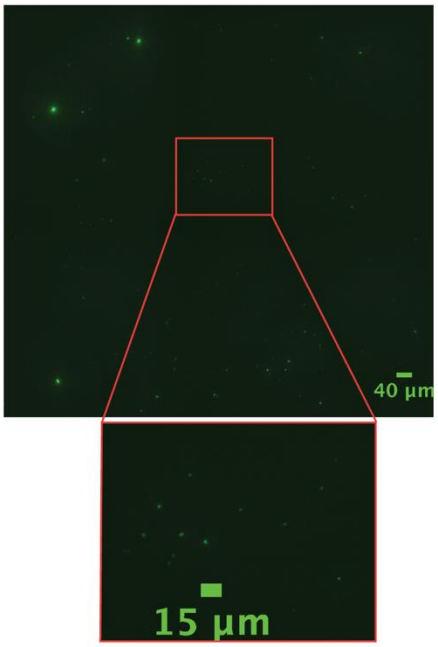

SI Figure 3 – PGN microparticles conjugate sfGFP only when both clickable handles are present and then allows for quantification. (A) Flow cytometry of modified and unmodified PGN microparticles reacted with modified and unmodified Cys3-sfGFP. Aza, azido-PGN microparticles; WT, “wildtype” PGN microparticles grown in the absence of D-aa. Comparing the mean fluorescence intensities of WT PGN microparticles (orange) and azaDala PGN microparticles (turquoise) yields the results in Figure 2b. (B) Example of a standard curve used to determine sfGFP concentrations in solutions of reacted PGN microparticles or KLH. (C) Confocal microscopy of sfGFP-reacted PGN microparticles plated on a blank slide. The image was used to count the number of spots (ImageJ) which, in combination with the concentration, allowed us to determine the sfGFP/PGN microparticle ratio.

SI Fig 4a

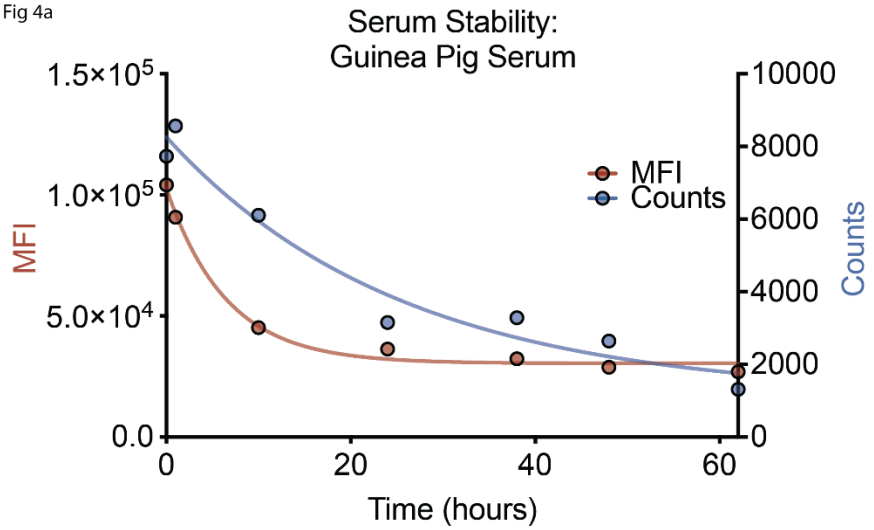

SI Fig 4b

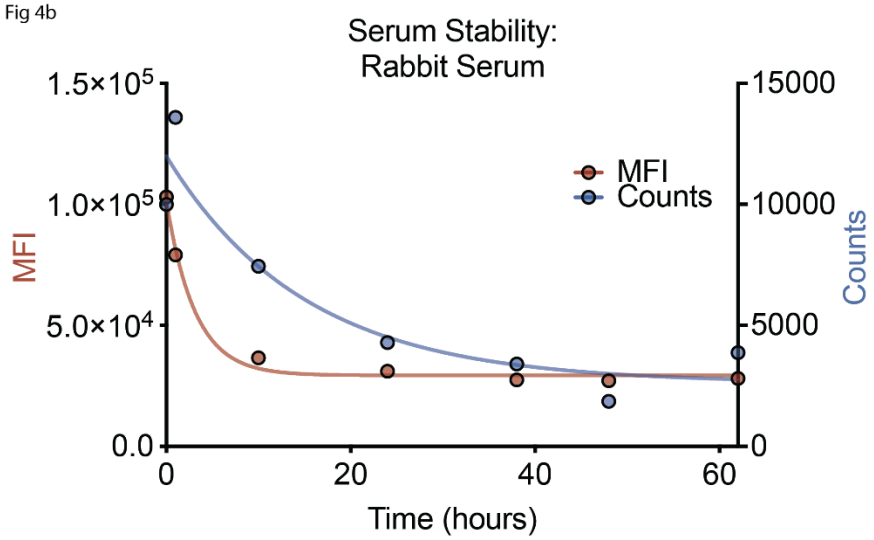

SI Figure 4. Stability of sfGFP-modified PGN microparticles in (A) guinea pig serum and (B) rabbit serum. Accuri flow cytometry was used to determine the number of PGN microparticles and mean fluorescence intensity (MFI; a measure of sfGFP fluorescence).

SI Fig 5a

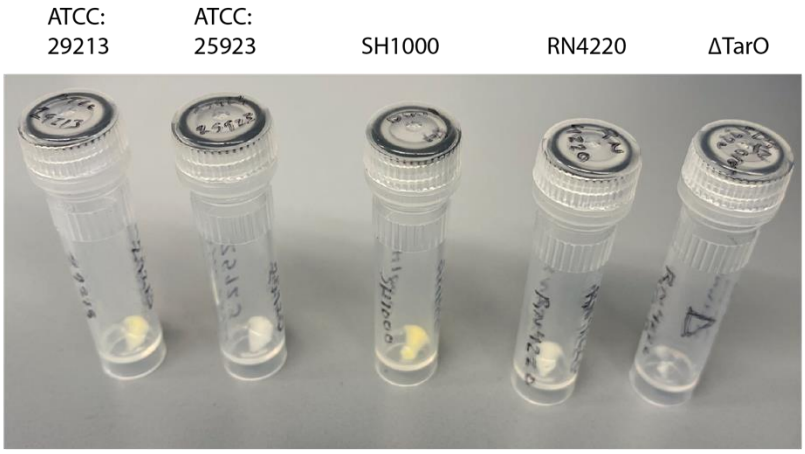

SI Fig 5b

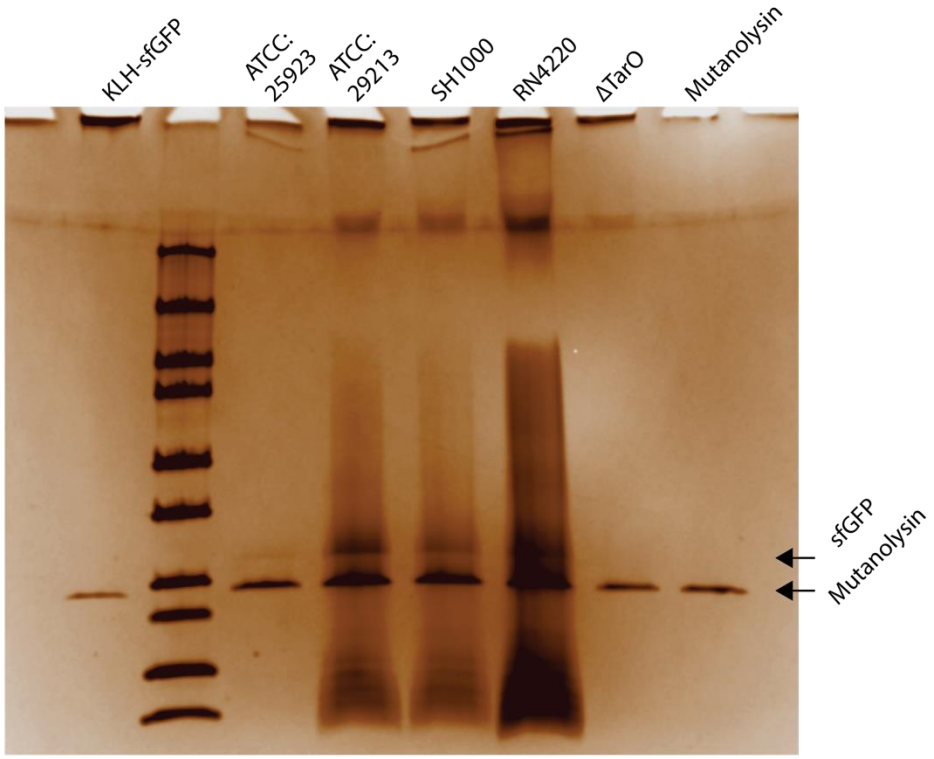

SI Figure 5. PGN microparticles isolated from different strains have a range of purity. (A) Photograph of isolated PGN microparticles from a variety of *S. aureus* strains. Note the difference in color between isolated PGN microparticles. (B) Silver stain of digested sfGFP-modified PGN microparticles and KLH-sfGFP.

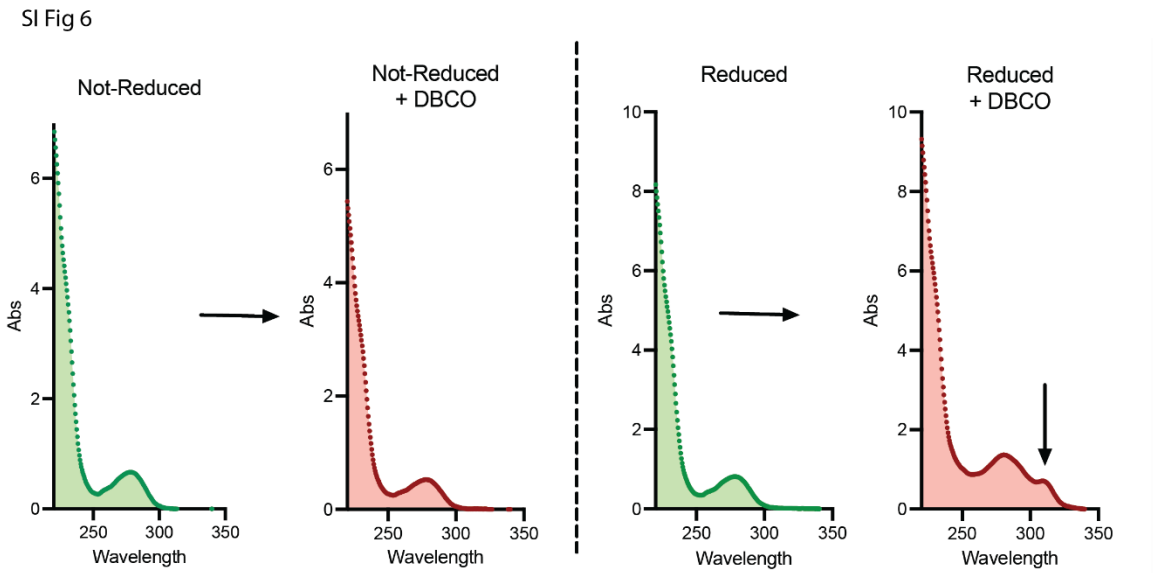

SI Figure 6 – UV absorbance spectra of SARS-CoV-2 RBD with the addition of maleimide-PEG$_4$-DBCO in the absence (left of dashed line) or presence (right of dashed line) of prior reduction. Unreduced or reduced SARS-CoV-2 RBD (green traces) was reacted with the maleimide-PEG$_4$-DBCO and then purified (red traces). DBCO absorbs light at 310 nm. Without reduction there was no reaction of SARS-CoV-2 RBD with the maleimide.

SI Fig 7

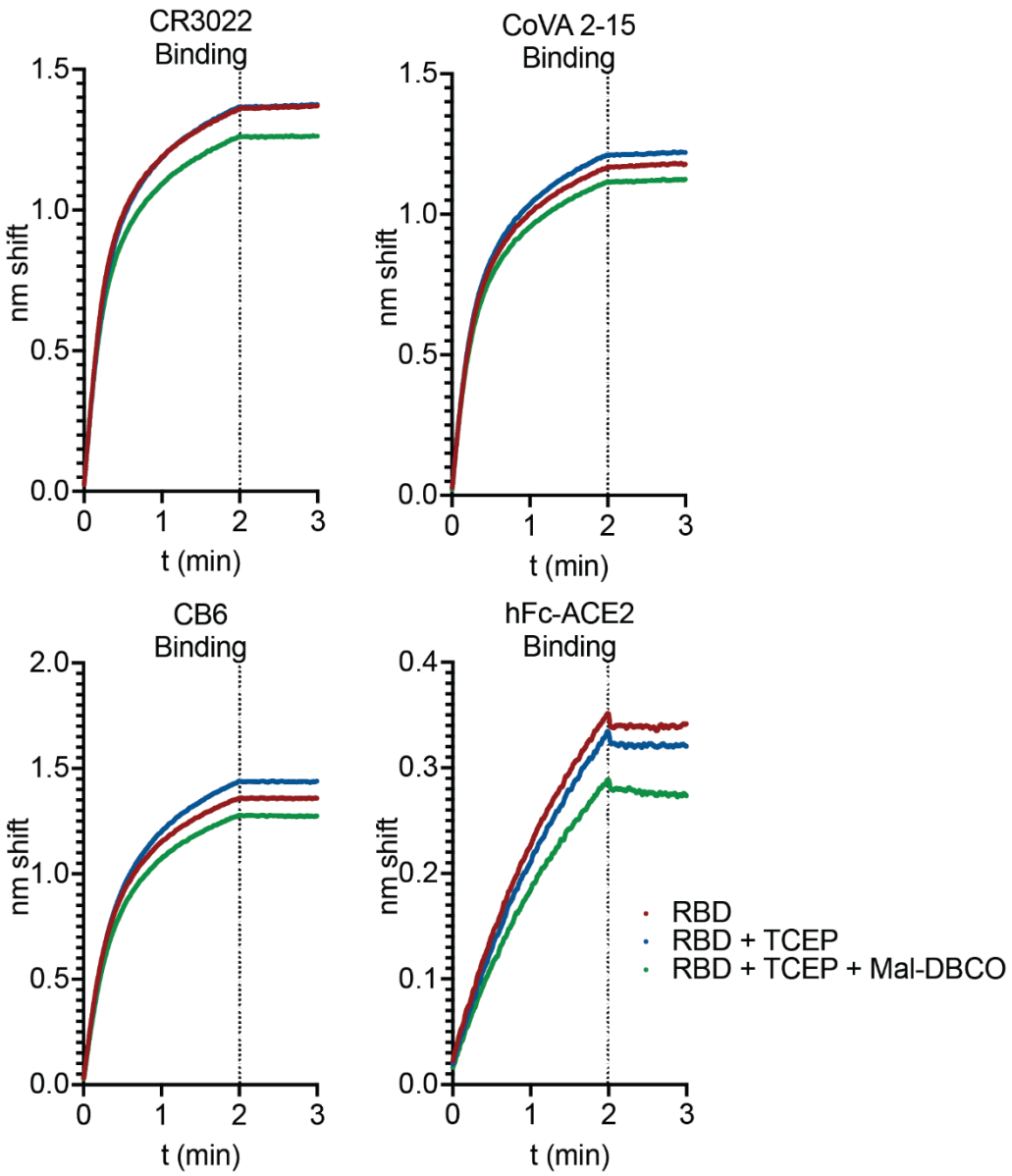

SI Figure 7 – Biolayer interferometry measurements of SARS-CoV-2 RBD before reduction, after reduction, and after maleimide-PEG_4-DBCO modification binding to three conformation-specific antibodies (CR3022, CoVA2-15, CB6) or hFc-ACE2. All curves demonstrate that reduction and modification did not substantially impact binding.

SI Fig 8

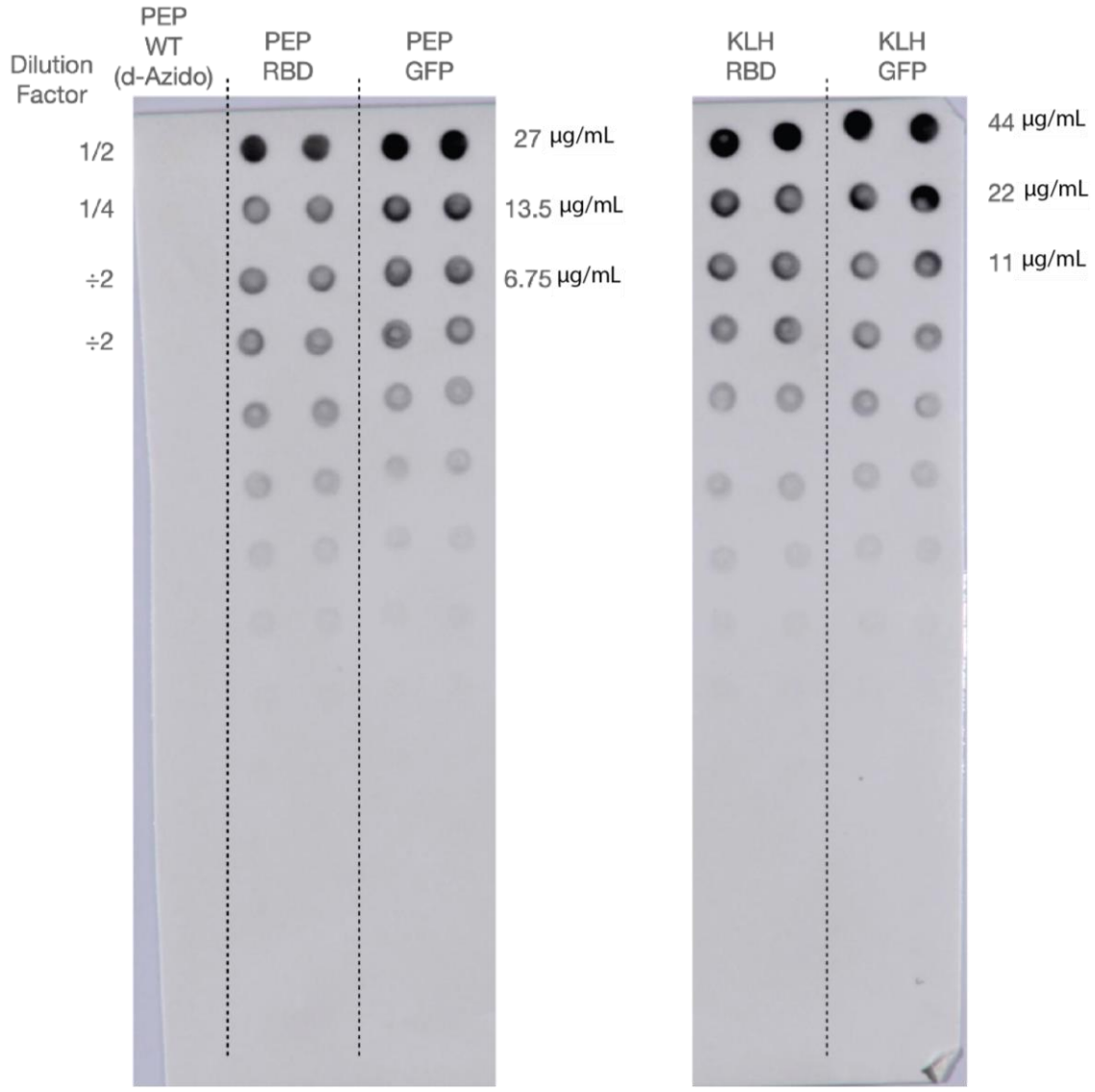

SI Figure 8 – Dot blot analysis allows for the quantification of RBD in the KLH and PGN microparticle samples. (Left) Anti-his tag dot blot of a dilution series of SARS-CoV-2 RBD-modified PGN microparticles (PEP RBD) and a dilution series of known sfGFP concentration of sfGFP-modified PGN microparticles (PEP GFP). The left lane contains unmodified PGN which is not detected on this blot. The relative intensity of the His-tag-specific antibody bridges the gap between sfGFP concentration and SARS-CoV-2 RBD concentration in this sample. (Right) Same dilution series but for KLH modified with SARS-CoV-2 RBD (KLH RBD) or sfGFP (KLH GFP).

SI Fig 8 Cont.

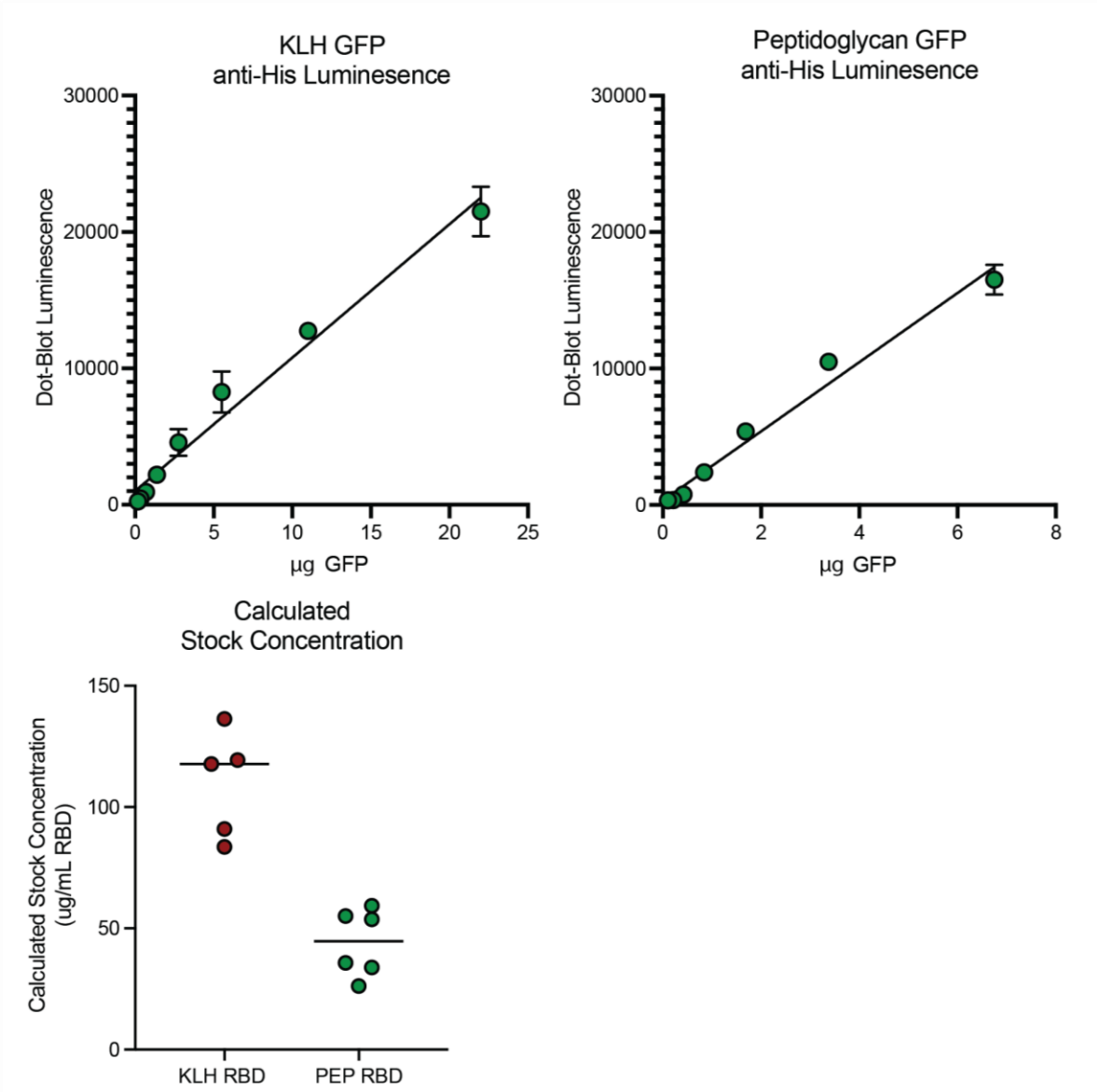

SI Figure 8 cont. (Top left) Luminescence intensity of the KLH dot blot in SI Figure 8 compared to the sfGFP concentration, allowing for the development of a standard curve. Curves were truncated when they fell outside the linear range. (Top right) Luminescence intensity of the PGN microparticle dot blot shown (n = 2) above compared to the sfGFP concentration, allowing for the development of a standard curve. Curves were truncated when they were outside the linear range. (Bottom) Standard curves were used to evaluate points of the dilution series calculated back to the stock based on their dilution factor (for example, the 4x dilution sample was multiplied by four). The average of these points (n = 6) was used to determine the concentration of SARS-CoV-2 RBD in the sample.